Universal conductance fluctuations in metals: Effects of finite temperature, interactions, and magnetic field

P. A. Lee
Department of Physics, Massachusetts Institute of Technology, Cambridge, Massachusetts 02139

A. Douglas Stone*
Department of Physics, State University of New York at Stony Brook, Stony Brook, New York 11794-3800

H. Fukuyama
Institute of Solid State Physics, University of Tokyo, 7-22-1 Roppongi, Minato-ku, Tokyo 106, Japan
(Received 9 July 1986)

The conductance of any metallic sample has been shown to fluctuate as a function of chemical potential, magnetic field, or impurity configuration by an amount of order e^2/h independent of sample size and degree of disorder at zero temperature. We discuss the relationship of these results to other results in the theory of weak and strong localization, and discuss its physical implications. We discuss the physical assumptions underlying the ergodic hypothesis used to relate theory to experiment. We review the zero-temperature theory and provide a detailed discussion of the conductance correlation functions in magnetic field and Fermi energy. We show that the zero-temperature amplitude of the fluctuations is unaffected by electron-electron interactions to lowest order in $(k_f l)^{-1}$, and at finite temperature interactions only enter insofar as they contribute to the inelastic scattering rate. We calculate the effects of finite temperature on both the amplitude of the fluctuations and their scale. We discuss the conditions for dimensional crossover at finite temperature, and the behavior of different experimental measures of the fluctuation amplitude, in order to facilitate quantitative comparisons of experiment and theory.

I. INTRODUCTION

Recent experimental studies[1,2] of the resistance of small metallic wires at low temperatures have revealed unexpected fluctuations as a function of magnetic field. These fluctuations are not noise in the usual sense, i.e., random, *time-dependent* changes in the resistance, but are time-independent stochastic magnetoresistance patterns ("magnetofingerprints") which vary between samples but are reproducible (at a given temperature) within a given sample. In small metallic rings such aperiodic structure in the magnetoresistance is seen as well, and in this case there are also h/e Aharonov-Bohm oscillations superimposed on this aperiodic background.[3-6] Quasi-one-dimensional metal-oxide-semiconductor field-effect transitions[7-10] (MOSFET's) in the metallic regime also show such aperiodic structure both in the magnetoresistance, and in the resistance as a function of chemical potential (gate voltage). Interestingly, the structure in gate voltage is typically of the same size as that in magnetic field; however, by varying gate voltage a recent study was able to rule out an interpretation where the magnetoresistance oscillations were simply due to field-dependent shifts in the electron energy levels.[7] The fluctuations disappear slowly and smoothly as temperature is increased in a given sample. Since the samples are very small this suggested that the fluctuations decrease as some temperature-dependent length scale becomes shorter than the sample dimensions. This in turn suggested that the sample-specific structure is a quantum interference effect which requires phase coherence in the wave functions (absence of inelastic effects) over large regions of the sample.

Theoretical investigations of these phenomena have shown that they are indeed a quantum interference effect characteristic of metals,[11] and the fluctuations have a universal $T=0$ amplitude of order e^2/h, independent of sample size and degree of disorder (as long as the sample is metallic).[12-14] The universality of the amplitude of the fluctuations at low temperature has been confirmed in a variety of quite different metallic systems (see Fig. 1). A key insight leading to the latter result was the realization that these sample-specific fluctuation phenomena in conductance versus magnetic field or chemical potential could be viewed as manifestations of the statistical fluctuations which would occur in the conductance of an ensemble of metallic samples which differed only in their microscopic impurity configurations. This idea made it possible to make a connection between analytic theoretical results, which typically average over a statistical ensemble, and experimental results which typically involve measurements on one or a small number of samples. In order to make such a connection an ergodic hypothesis of a certain type was assumed[13,14] which will be discussed in some detail below. In this paper we review and augment the zero-temperature theory of these fluctuations, show that they are insensitive to interaction effects, and extend the theory to finite temperatures. This should allow detailed quantative comparison between theory and experiment.

It has long been recognized that the conductance exhib-

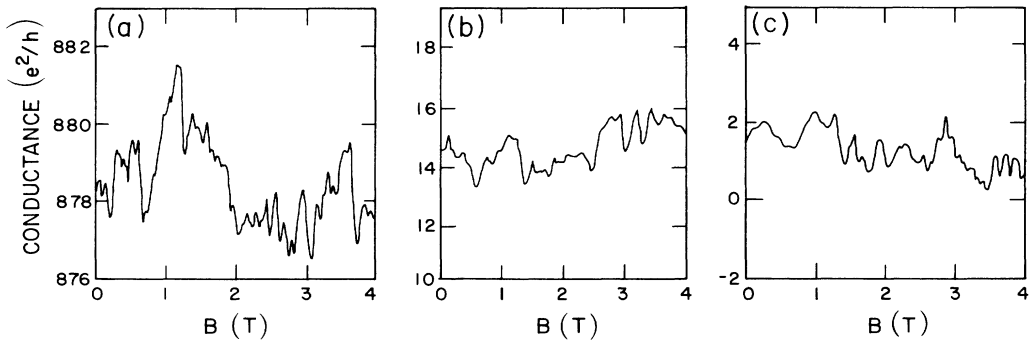

FIG. 1. Comparison of aperiodic magnetoconductance fluctuations in three different systems. (a) $g(B)$ in 0.8-μm-diam gold ring, analysis of data from Refs. 3 and 4, reprinted with the permission of Webb *et al.* (the rapid Aharonov-Bohm oscillations have been filtered out). (b) $g(B)$ for a quasi-1D silicon MOSFET, data from Ref. 9, reprinted with the permission of Skocpol *et al.* (c) Numerical calculation of $g(B)$ for an Anderson model using the technique of Ref. 11. Conductance is measured in units of e^2/h, magnetic field in tesla. Note the 3 order-of-magnitude variation in the background conductance while the fluctuations remain order unity.

its large statistical fluctuations when the sample size exceeds the localization length. Most of the work on statistical fluctuations has examined purely one-dimensional (1D) disordered systems;[15–19] and is based on evaluation of the 1D Landauer formula[15] for the dimensionless conductance, g (conductance G in units of e^2/h) of a quantum resistor

$$g=\frac{G}{e^2/h}=\frac{2|t|^2}{1-|t|^2}\ , \tag{1.1}$$

where $|t|^2$ is the transmission coefficient of the resistor, which is treated as a single scattering region between perfectly ordered "leads." In the 1D strongly-localized case it was shown that the fluctuations are so large that $\ln g$, and not the conductance g has a normal distribution.[16–19] A consequence of this is that for a system of length L, $\mathrm{Var}(R)/\langle R\rangle^2\sim\exp(\lambda L)$ (λ is a constant of order unity), i.e., the relative variance of the resistance actually diverges exponentially as the length of the system goes to infinity. Hence not only was the resistance a non-self-averaging quantity in the thermodynamic limit, it was actually statistically pathological. It was pointed out at the time that such exponentially large fluctuations should not be observable in metallic systems, where the quantum corrections to the conductance were cut off by the inelastic scattering length.[20] The first step towards relating these statistical fluctuations to experiment was taken as a result of work by Lifshitz and Kirpichenkov,[21] and Azbel and co-workers,[22,23] who also suggested a simple physical reason for the presence of large fluctuations in the conductance. For a strongly-localized 1D system at typical energies the transmission coefficient would be exponentially small, $|t|^2\sim\exp(-2L/\xi)$, where ξ is the localization length, and L is the sample length. However, nearby an energy where (for a closed system) there would exist a localized state close to the center of the sample, an incident electron can resonantly tunnel through the sample via this localized state with a probability approaching unity. The width Γ of such a resonance in energy is, however, exponentially narrow, $\Gamma\sim\exp(-L/\xi)$ thus the conductance as a function of energy exhibits large narrow spikes above the background nonresonant transmission. Moreover, the particular spectral pattern of conductance versus Fermi energy (or chemical potential at finite temperature) would be characteristic of a single sample, and its particular impurity configuration. This is perhaps the most novel feature of these quantum fluctuation phenomena in general, since it violates the usual assumption of transport theory, that a given sample is well described by the average behavior. These large fluctuations of the conductance of a single sample versus energy could be regarded as a reflection of the large statistical fluctuations expected from sample to sample at a fixed energy, assuming that changing a continuous parameter upon which g depends (the energy) is equivalent to changing the impurity configuration at fixed energy. To our knowledge there exists no proof that this is quantitatively correct for the strongly-localized case,[24] but the presence of large statistical fluctuations and large fluctuations in g versus energy is suggestive. The actual experimental behavior of 1D MOSFET's may not reflect these resonant tunneling fluctuations, because at finite temperature other conduction mechanisms, such as Mott variable-range hopping may dominate,[25,26] which also have interesting associated fluctuation phenomena.[27]

In this paper we are interested in fluctuation phenomena that occur in the metallic regime. We define a metal as a conductor in any dimension whose sample dimensions are much greater than the elastic mean free path but less than the localization length; or equivalently one may say any sample much longer than the elastic mean free path whose $T=0$ conductance is much greater than e^2/h. By a famous argument due to Thouless[28] one can see that this corresponds to the opposite limit from the resonant tunneling picture of the strongly-localized regime. Thouless argued that the energy levels of a metallic sample (where the motion is diffusive) should be uncertain due to boundary effects by an amount inversely proportional to the time to diffuse across the sample, L^2/D, where D is the elastic diffusion constant. It is natural to associate the uncertainty in the energy levels of a closed sample due to boundary effects with a decay or resonance width, hence for a metal

$$\Gamma_M \simeq hD/L^2 . \tag{1.2}$$

Moreover, for a metal this decay width is simply related to the dimensionless conductance. If we consider the ratio of Γ_M to the average level spacing $W=(N_0L^d)^{-1}$, where N_0 is the density of states, we find

$$\Gamma_M/W = N_0 D L^{d-2} = \sigma L^{d-2}/(e^2/h) = g , \tag{1.3}$$

where σ is the conductivity, and we have used the Einstein relation. Thus we see that the condition $g>1$ which defines the metallic regime, is equivalent to the condition that the resonance width is larger than the level spacing, and so the metallic regime corresponds to the opposite limit from the narrow, well-separated resonances expected in the strongly-localized regime. Thus we expect the exponentially large fluctuations in g versus E to subside once the states become extended, but we do not expect them to disappear entirely, and the quantitative statistical behavior of such a system as the sample dimensions become very large was, until recently, entirely an open question. We now know that metallic systems exhibit a statistical behavior as a function of sample size which is intermediate between the self-averaging of classical resistor networks (to be discussed below), and the divergent fluctuations characteristic of strongly-localized systems. In addition, in the metallic regime the absolute fluctuations in g have the universal, disorder, and size-independent behavior described above. Since $\mathrm{Var}(g)$ is found to be size independent in all physical dimensions, the question of whether the conductance self-averages becomes dimensionally dependent. A system variable is usually said to self-average only if its *relative* variance goes to zero as the system size goes to infinity. Since by Ohm's law the average metallic conductance scales as L^{d-2}, we have

$$\mathrm{Var}(g)/\langle g\rangle^2 \sim L^{2(2-d)} .$$

This means that the conductance of a metal self-averages in three dimensions, but not in one or two (and even in three dimensions the relative variance decreases more slowly than the inverse volume dependence expected classically). Of course if one scales a metal in one and two dimensions the scaling theory of localization[29] predicts that it will always cross over eventually to strong localization and hence to the regime of exponentially large relative fluctuations.

In order to extend the analysis of statistical fluctuations to the metallic regime it was essential to generalize the 1D models studied in the strongly-localized regime to higher dimension (in the above discussion of metallic scaling our argument really only applied to quasi-one-dimensional systems). That is because in a purely 1D quantum system there is no true metallic regime, since the localization length is essentially equal to the elastic mean free path.[30] Therefore the transport is either ballistic or localized, whereas in a metal it is diffusive, the electron performing a random walk of step length l (the elastic mean free path) on length scales smaller than ξ at $T=0$. To accomplish this generalization we calculate the conductance of electrons in the following system: a finite disordered region of volume $V=L_x^{d-1}L_z$, extended to $\pm\infty$ in the z direction by attaching ideal "leads," with an electromagnetic field applied only to the disordered region. The dimensionless dc conductance including spin at $T=0$ is[31]

$$g = \left(\frac{2\pi}{L_z}\right)^2 \sum_{\alpha,\beta} \left| \int_V d\vec{r}\, \frac{1}{2im} \left(\frac{\partial\psi_\alpha^*}{\partial z}\psi_\beta - \psi_\alpha^* \frac{\partial\psi_\beta}{\partial z} \right) \right|^2 \times \delta(E_F-E_\alpha)\delta(E_F-E_\beta) , \tag{1.4}$$

where E_F is the Fermi energy, ψ_α and E_α are the exact eigenstates and energies of the disordered region plus leads, and the integral is only over the volume of the disordered region. Effects of a magnetic field may be included simply by calculating these eigenstates in the presence of a field. As is true in the 1D case, the transport of electrons through the disordered region can be considered as a scattering problem where electrons from the leads are transmitted or reflected by the random potential. It was also shown[31] that Eq. (1.4) is equivalent to the relation

$$g = 2\,\mathrm{Tr}(\underset{\sim}{t}\,\underset{\sim}{t}^\dagger) , \tag{1.5}$$

where $\underset{\sim}{t}$ is the transmission matrix through the disordered region, which connects the various states of transverse momentum on one side of the disordered region with those on the other side.

Equation (1.5) is one possible generalization of the 1D Landauer formula of Eq. (1.1) to a many-channel (higher-dimensional) system. The issue of how to correctly generalize the 1D formula to the many-channel case is a complicated problem which has generated much discussion.[31–34] However, in the metallic regime, where the sample dimensions are much greater than l, Eq. (1.5) is found[11] to have similar features to other proposed multichannel Landauer formulas, and is an appropriate starting point. It is still an open question whether Eq. (1.5) is quantitatively accurate in the metallic regime (up to corrections of order l/L), but it is encouraging that ensemble averaging Eq. (1.5) does give exactly Ohm's law in the large system limit. Moreover, it is very important to appreciate that all the multichannel Landauer formulas proposed give the conductance as a relatively simple function of the elements of the scattering matrix of the disordered region. Hence, in general, the problem of quantum transport can be treated by the techniques of scattering theory and is seen to be closely related to well-studied problems in other subdisciplines of physics, particularly nuclear physics. This illustrates the power and utility of the Landauer approach which considers transport as a consequence of incident carrier flux.[35]

It is therefore worth pointing out an intriguing analogy between the fluctuation phenomena in quantum transport that we are addressing, and similar fluctuation phenomena in the scattering cross sections of heavy nuclei. Many years ago Bohr proposed[36] the idea that in collisions of nucleons with complex heavy nuclei a compound nucleus is briefly formed and the resulting energy levels of the combined system are responsible for the multitude of observed scattering resonances. The idea of a statistical treatment of these compound nuclei was then proposed,[36–39] in which the compound nucleus was described by a random Hamiltonian, and each nucleus was supposed to be a particular member of a given ensemble of random

Hamiltonians, classified by their symmetries. Of course the fluctuations between the spectra of various ensemble members were not assumed to be negligible; each nucleus has a unique distinguishable spectrum. As noted above, condensed-matter physics has now entered a similar regime in transport theory, where each sample has a particular behavior which is not well described by the ensemble-averaged behavior. At low energies the resonances of the compound nuclei are narrow and well resolved, just as they are in the resonant tunneling picture of the strongly-localized regime. Much work has gone into deriving a statistical picture of this low-energy regime, which, because of the phenomenon of level repulsion, was found to have some novel statistical properties typical of objects whose behavior is statistically correlated. At higher energies the resonances in the scattering cross section broaden until they eventually overlap, just as they do in our picture of the metallic regime. In this high-energy regime there are only small oscillations in the scattering cross section as a function of energy. These high-energy fluctuations have been described by Ericson and Mayer-Kuckuk,[40] who showed that the typical scale of the fluctations (the energy correlation range) was given by the average resonance width and was independent of the average spacing. An analogous result for the energy correlation range of the metallic conductance was proved in Ref. 13.

Although there appears to be a strong analogy between the low-energy and high-energy regimes in the statistical treatment of the nucleus, and the strongly-localized and metallic regimes in quantum conduction, the analogy is not complete, for at least two reasons. Most importantly, the connection between sharp resonances and localized states on the one hand, and broad, overlapping resonances and extended states on the other, which is a crucial feature of the quantum conduction problem, does not carry over to the nuclear problem. In the compound nucleus, even in the low-energy regime the nuclear eigenstates must be extended in the relevant sense. This is known because empirically the spectra do exhibit the statistical behavior characteristic of level repulsion and of long-range spectral rigidity. This latter property means that the fluctuations in the number of levels in a given energy interval are essentially independent of the size of that interval, instead of increasing as the square root of the size as expected for uncorrelated (Poisson-distributed) objects. Whereas for states spatially localized in different regions there is little overlap and hence negligible level repulsion, the spectrum should be well described statistically by a Poisson distribution of levels. The reason the "extended" nuclear eigenstates give rise to sharp resonances anyway is presumably because the coupling to outside channels is dominated by some effective potential barrier, so that the decay rate is much smaller than that given by the inverse time to diffuse to this boundary. Hence the low-energy nuclear behavior is more closely analogous to the behavior of a metallic conductor with a large contact resistance. Therefore it is possible that the theory of the statistical behavior of random matrices which has been successfully applied to the sharply resonant regime of compound nuclei does have relevance to the description of fluctuations in metallic conduction; although in the latter case one is not simply dealing with the energy levels of a random Hamiltonian but rather a scattering (or transfer) matrix which also contains spatial information about the wave functions. Indeed a recent argument by Imry[41] derives the universality of the metallic conductance fluctuations based on the assumption that the transfer matrix across the disordered region (which is related to the inverse of the transmission matrix) exhibits this eigenvalue rigidity characteristic of nuclear spectra. It is interesting to note that from this point of view the e^2/h fluctuations in g are actually *smaller* than would be expected based on the simple assumption of a Poisson distribution of eigenvalues for the transfer matrix; whereas from the more familiar point of view of classical transport theory (to be explained shortly) the fluctuations are much larger than expected. Very recently, Al'tshuler and Shklovskii[42] have made a detailed analysis of the level statistics of small metallic systems and shown that while the spectrum exhibits Dyson-Mehta rigidity over some range in energy,[43] the overall band exhibits much larger fluctuations. Hence they showed that the occurrence of universal, size-independent fluctuations in the square of the transmission matrix is not equivalent to spectral rigidity of the random Hamiltonian; this is of course consistent with Imry's argument which assumes the transfer matrix, and not the Hamiltonian itself, exhibits eigenvalue rigidity. On the other hand, by direct evaluation of the variance of the density of states, Al'tshuler and Shklovskii were able to show that at zero temperature a finite fraction of the variance of the conductance comes from density-of-states fluctuations; a result which is appealing because it implies that one can think of the universal conductance fluctuations as arising from fluctuations in the number of resonances contained within an energy interval equal to the typical resonance width. Thus, although similar in spirit, the statistical behavior of these metallic systems does appear to be rather different from that described in the statistical theory of nuclear spectra.

A second difference between the nuclear scattering and quantum conduction problems is that the relevant eigenstates of the compound nucleus are many-body wave functions, and the random Hamiltonian is defined in a many-particle Hilbert space. Thus the concept of single-particle diffusion in real space, which is central to the behavior of the conductance fluctuations, has apparently no counterpart in the nuclear-physics problem. Therefore the universal amplitude of the conductance fluctuations is probably not relevant for calculating the amplitude of Ericson oscillations.

To appreciate the special quantum-mechanical nature of the conductance fluctuations, it is useful to contrast their behavior with that of a network of classical resistors with random resistances. In one dimension the statistics of such a network is trivial. The total resistance is the sum of the N resistances, $R=\sum_{i=1}^{N} r_i$; therefore, by the central limit theorem

$$\mathrm{Var}(R)/\langle R\rangle^2 \sim \mathrm{Var}(r)/N\langle r\rangle^2$$

[where $\mathrm{Var}(R)=\langle (R-\langle R\rangle)^2\rangle$]. Since the length of the total network is proportional to N, the relative variance

decreases as $1/L$. If the fluctuations in each resistor are small compared to the mean resistance, the same result applies for the conductance. Since even in higher dimension the classical conductance is essentially an additive function of the constituent conductances, this result generalizes to higher dimension, and it can be shown that far away from the percolation threshold a classical network obeys

$$\frac{\mathrm{Var}(g)}{\langle g\rangle^2}\sim\frac{1}{L^d}\ . \tag{1.6}$$

Thus the conductance classically self-averages in the same way as do thermodynamic fluctuations around thermal equilibrium. For a metal, where the conductance obeys Ohm's law, $\langle g\rangle\sim\sigma L^{d-2}$, Eq. (1.6) implies

$$\mathrm{Var}(g)\sim L^{d-4}\ . \tag{1.7}$$

Thus, for a classical metallic system, in all dimensions less than four the absolute variance goes to zero as some power of the system size. As noted above, the results of Refs. 12–14 show that for a quantum-mechanical metallic system Var(g) is order unity in all dimensions less than four. However, it is now well understood due to work of Thouless[30] that at finite temperature the transport properties of a metal behave classically on length scales larger than the inelastic diffusion length $L_{\mathrm{in}}=(D\tau_{\mathrm{in}})^{1/2}$, where τ_{in} is the inelastic scattering rate, because the electron is likely to experience a dynamic interaction which erases phase memory beyond this scale. Therefore, when a metallic sample is studied at temperatures where L_{in} is much less than the sample dimensions (which is always the case for a macroscopic sample), we expect

$$\mathrm{Var}[g(T)]\sim\mathrm{Var}[g(L_{\mathrm{in}})](L_{\mathrm{in}}/L)^{4-d}\ ,$$

where $\mathrm{Var}[g(L_{\mathrm{in}})]$ is the variance at scale L_{in}. In the simplest case $\mathrm{Var}[g(L_{\mathrm{in}})]$ is just the order unity $T=0$ result (however, as we shall see in Sec. IV, there are other thermal effects which can reduce it somewhat below the $T=0$ value).

The onset of classical self-averaging at scales larger than L_{in} explains why it is easiest to observe these fluctuation effects in systems on the "mesoscopic" size scale, since L_{in} is typically a few microns at the lowest experimentally accessible temperatures. Nonetheless, as we will see in Sec. III, the classical self-averaging of the amplitude is such a weak function of temperature that it definitely should be possible to observe these fluctuations effects in the low-temperature conductance of samples much larger than the inelastic length. The main reason the effects are not seen in room-temperature magnetoresistance is that the field range needed to observe these fluctuations becomes too large (see Sec. III). However, other manifestations of these fluctuations may be observed at room temperature (or at least at temperatures much higher than 1 K). Very recent work[44] has suggested that such fluctuations induced by small changes in the impurity configuration may be the microscopic origin of $1/f$ noise in dirty metallic systems. Moreover, it should be clearly understood that if one takes the existence of sample-specific fluctuations as a criterion of the mesoscopic regime, then mesoscopic size is only defined relative to the temperature at which one is observing the system. In principle, these effects can be observed in truly macroscopic systems at low enough temperature.

Having seen that the size-independent behavior of the $T=0$ fluctuations implies a failure of the classically expected self-averaging, it is instructive to consider how this behavior compared to an estimate of the fluctuations expected quantum mechanically, based on making the simplest assumptions possible about the statistical properties of the transmission coefficients $|t_{ij}|^2$ appearing in Eq. (1.5). Here we follow the spirit of the discussion by Büttiker *et al.*,[34] who were the first to emphasize the importance of possible non-self-averaging behavior in considering the Aharonov-Bohm effect in normal-metal rings. An earlier paper by Gefen, Imry, and Azbel,[45] had shown that there were Aharonov-Bohm oscillations in the conductance of purely 1D (one-channel) rings with fundamental period h/e and sample-specific shape. They suggested that such an effect could be seen experimentally despite the possible self-averaging which was expected to occur between the many different channels of a true metal ring. Büttiker *et al.* considered directly the many-channel case and attempted to estimate the self-averaging of different contributions from each channel to the h/e Aharonov-Bohm oscillations in a metal ring, which it turns out have a statistical behavior similar to the aperiodic fluctuations[13,14,46,47] we have been discussing. We have (for one spin channel)

$$g=\mathrm{Tr}(\underset{\sim}{t}\,\underset{\sim}{t}^{\dagger})=\sum_{i,j=1}^{N_c}|t_{ij}|^2\ , \tag{1.8}$$

where i and j are channel indices, and N_c is the total number of channels, which is proportional to the cross-sectional area [typically $N_c\sim(wk_F)^{d-1}$, where w is the width]. Denote $|t_{ij}|^2=T_{ij}$, and suppose that each $T_{ij}=\sum_{\alpha,\beta}C_\alpha C_\beta^*$, where C_α are complex amplitudes which we will discuss in more detail below. Suppose that the number of terms in the sum $N_p\gg1$, then if the moduli of the C_α are comparable but the phases are uncorrelated it is easily seen that

$$\mathrm{Var}(T_{ij})/\langle T_{ij}\rangle^2\simeq1 \tag{1.9}$$

up to corrections of order N_p^{-1}. It is also easy to check that if some of the amplitudes have correlated phases this result still holds except the corrections are now of the order of the inverse of the number of uncorrelated phases. Therefore under rather general conditions the relative variance of an individual transmission coefficient is order unity, and this is an essentially trivial effect which requires no subtle statistical correlation of phases.

Thus following these simple assumptions, we can write each T_{ij} as $T_{ij}=T_0+\delta T_{ij}$, where T_0 is the ensemble-averaged value of the transmission coefficient for a single channel (assumed not to vary much from channel to channel), and δT_{ij} is the deviation from the average, which can of course have either sign, and which has an rms deviation of order T_0. If we now assume that the different δT_{ij} are uncorrelated, then [denoting the conductance fluctuations obtained under these assumptions by $\mathrm{rms}(g_u)$], $\langle g\rangle=N_c^2T_0$, whereas $\mathrm{rms}(g_u)\simeq N_cT_0$. Hence

we would expect

$$\mathrm{rms}(g_u) \simeq \langle g \rangle / N_c \ . \tag{1.10}$$

Since the average Boltzmann conductivity can be written as $\sigma = (e^2/h) k_F^{d-1} l$ and Ohm's law gives

$$\langle g \rangle = [\sigma/(e^2/h)] \frac{w^{d-1}}{L} \ ,$$

we find

$$\mathrm{rms}(g_u) \simeq \frac{l}{L} \ . \tag{1.11}$$

Therefore the assumption of uncorrelated fluctuations in each conduction channel in Eq. (1.5) is incorrect, as it gives an answer which is smaller (typically by a rather large factor) than the correct answer $\mathrm{rms}(g) \simeq 1$. If this estimate were correct the fluctuation effects would usually be negligible compared to the weak localization interference effects in the average conductance, even at $T=0$, and in general the quantum effects in the conductance would be well described by the ensemble-averaged behavior. Büttiker *et al.* were led to Eq. (1.10) by similar reasoning, and they explicitly noted that this result was not necessarily a good order-of-magnitude estimate, but simply a reasonable lower bound on the size of the fluctuating h/e contribution. It is an interesting lower bound for two reasons. First, it suggests the presence of statistical fluctuations which even by Eq. (1.11) are typically larger than those predicted by classical self-averaging. Secondly it points to the fact that some sort of spatial correlation in the statistical behavior of the wave functions is required to explain the universal magnitude of the conductance fluctuations. It has been recognized for some time that[48] quantum diffusion imposes a long-range spatial correlation between wave functions. This correlation plays a crucial role in enhancing the effect of interactions in dirty metals, and the results of Refs. 12 and 13 show that the same effect manifests itself in enhancing the conductance fluctuations. This point will be discussed further in the next section. Finally, based on similar considerations to those above, Imry[41] has recently pointed out that while the true physical conduction channels must be correlated to give the universal value for the conductance fluctuations [and not (1.10)], one may interpret this as implying that there is an effective number of uncorrelated, active conduction channels that changes in a well-defined manner with the system dimensions and degree of disorder.

Having discussed various aspects of the statistical fluctuations, we now return to their relation to the conductance fluctuations as a function of magnetic field or chemical potential within a given sample. We have hypothesized that the behavior of these sample-specific fluctuations (as a function of size, disorder, etc.) is the same as the statistical fluctuations obtained by varying impurity configuration. The heuristic physical argument which underlies this "ergodic" hypothesis is the following: the transmission coefficients $|t_{ij}|^2$ appearing in Eq. (1.5) for g are simply related to the probability $|G(0,L,\underline{r}_1,\underline{r}_2,E)|^2$ to propagate from a point $(z=0,\underline{r}_1)$ on one side of the disordered region to a point $(z=L,\underline{r}_2)$ on the other side (G is the Green function).[31] The (energy) Green function can be expressed as a path integral which is dominated by the classical trajectories at energy E between the two points (in WKB approximation, which should be sufficient to give the qualitative behavior). Then

$$|G(0,L,\underline{r}_1,\underline{r}_2)|^2 = \sum_{p,p'=1}^{N_p} A_p A_{p'} \exp(iW_p - iW_{p'}) \ , \tag{1.12}$$

where $W_p = S_p - Et_p$, and S_p is the action along classical trajectory p between $(0,\underline{r}_1)$ and $(L,\underline{r}_2)$ traversed in a time t_p, and A_p is the amplitude (given by a fluctuation determinant) for traversing the path p.[49] N_p is the number of classical (random-walk) trajectories traversing the disordered region, which we do not attempt to calculate explicitly. If we consider two paths p and p' in Eq. (1.12) such a pair forms a closed loop which returns to $(0,\underline{r}_1)$, and in the presence of a magnetic field the total phase in the exponent $W_p - W_{p'}$ acquires an additional relative phase $2\pi\Phi_{pp'}/\Phi_0$, where $\Phi_{pp'}$ is the flux enclosed by the loop, and $\Phi_0 = h/e$.

Now, in general, the phases $W_p, W_{p'}$ in the exponent have an arbitrary relationship for two different paths p and p', even in the absence of a field. Thus the contributions from the cross terms (interference terms) in Eq. (1.12) are expected to ensemble average to zero, leaving only a contribution from $p=p'$, which would of course be insensitive to small magnetic fields. The weak localization negative magnetoresistance arises because there exists a special subset of trajectories, time-reversed pairs which form a closed loop[50–52] (two paths where exactly the same scattering sequence is traversed but in opposite order) which always have a fixed relative phase ($W_p = W_{p'}$ at zero field) for any impurity configuration. Such trajectories make a coherent contribution which decreases the transmission at zero field (increases the backscattering) compared to the average value expected by ignoring interference terms in Eq. (1.12), and which *does not average to zero.* In a multiple-connected Aharonov-Bohm geometry, these time-reversed pairs make a contribution to the average conductance which oscillates with period $h/2e$.[53,54] In general, the configuration-independent interference effects of this type give rise to the weak localization effects in the average conductance, which have been extensively studied, both experimentally and theoretically since the work of Abrahams *et al.*[29] At zero temperature these average effects are also corrections of order e^2/h independent of size (in one dimension, and in two dimensions up to logarithmic corrections).

On the other hand, there is another configuration-*dependent* interference effect whose presence is indicated from Eq. (1.12), but which would never contribute to the ensemble-averaged conductance, and which thus was ignored until recently. That is the incoherent interference of all the paths with no fixed relative phase; there are N_p^2 such terms in Eq. (1.12) which by the argument sketched above in connection with Eq. (1.10) would expect to give an rms effect of order N_p *for a given impurity configuration* (set of paths), although, as noted above, such a contribution will ensemble average to zero. Even if some of the paths have correlated phases, as long as many paths contribute to the sum with approximately equal weight, the

phase-sensitive terms must make at least as large a contribution to the fluctuations as the phase-insensitive terms. However, if one path dominates the sum, then the fluctuations in the amplitude to traverse the best path will be most important. It is plausible that many paths have similar amplitude in the metallic regime where the states are extended; hence in the metallic regime the dominant fluctuation effect is likely to come from the stochastic interference of many classical trajectories which traverse the sample. In the strongly-localized regime it is not at all clear that many paths contribute and the physical origin of the fluctuations may be different. It is therefore quite possible that for strongly-localized systems changing magnetic field will not be equivalent to changing impurity configuration.

However, this picture suggests that the primary cause of the fluctuations from sample to sample in the metallic regime is that changing impurity configuration alters the phases in Eq. (1.12) in an arbitrary manner, causing the interference terms to vary chaotically. But if this is correct, one can equally well alter these phases with a given impurity configuration, simply by imposing a magnetic field and introducing a further, arbitrary relative phase to each pair of paths. Of course one must change the field enough that the dominant paths experience a relative phase change of order 2π, and this leads naturally to the idea that there is some *field correlation range* beyond which the phases become uncorrelated (in a fixed, static manner) with those at the original value of the field. It further suggests that this scale is set by the field at which the flux through the normal area of the sample is of order $\phi_0 = h/e$, based on the simple assumption that typical pairs of paths across the sample enclose roughly the sample area. This is in fact the result which was obtained first numerically[11] and then analytically.[13,14] A similar argument shows that the rms amplitude of the h/e Aharonov-Bohm effect in metal rings is determined by a random interference effect of this type,[46,47] and hence has the same statistical behavior.

Similarly, one can alter the phase change in traversing a given sample by changing the energy at which the particles traverse the disordered region. Suppose one assumes that to lowest order changing the energy does not affect the action along the path, or the time it takes to traverse the path, but simply changes the phase accumulated along that path, so that

$$W_p(E+\Delta E) = S_p - (E+\Delta E)t_p \ .$$

Since these classical paths are typically random-walk trajectories with diffusion constant D, the times involved are typically the times to diffuse across the sample, $t_p \simeq L^2/D$. Thus the energy change needed to randomize a given phase W_p is simply $\Delta E \sim hD/L^2$, which is the correct result for the *energy correlation range* obtained more rigorously below. Different arguments for this result have been given independently by Imry *et al.* (see Refs. 47 and 55). Although this heuristic path integral approach is helpful in justifying our ergodic hypothesis and gives the correct correlation lengths, one must be careful of extending the approach naively. If one considers the problem on a 2D lattice which is N sites wide (so that there are approximately N transverse conduction channels) then there are N^2 matrix elements of the Green function which connect points on the two different sides of the disordered region. The conductance is given by a linear combination of these N^2 matrix elements; hence assuming they all fluctuate independently would immediately lead us back to Eq. (1.10). Therefore these matrix elements cannot be statistically independent, which again leads to the conclusion that some sort of spatial correlation in the wave functions is necessary to give the universal amplitude of the conductance fluctuations.

Since the rms amplitude of the fluctuation effects is found to be e^2/h, independent of size or degree of disorder at $T=0$, they can often be as large or somewhat larger than the weak localization effects (this will be discussed in detail in Sec. II), although they do not have the same physical origin, as is clear from the above discussion in terms of Feynman paths. Thus under certain circumstances, which can be easily realized in small samples at low temperature, weak localization theory fails to provide a good description of the behavior of the conductance of a metal in the low-temperature limit, in the sense that for any given sample the fluctuation effects are typically as large or larger than the average effects, and mask this behavior. At higher temperatures and in larger samples, the classical self-averaging effects which occur on scales much longer than L_{in}, attenuate the fluctuation effects and thus make it possible to obtain good agreement between weak localization theory and experiment, even in one and two dimensions.

To summarize, this heuristic argument, in which the fluctuations are interpreted as a stochastic interference effect, suggests the hypothesis that for a metal equivalent fluctuations are caused by changing impurity configuration, or by changing magnetic field or energy within a given sample. Numerical and analytic calculations strongly support this hypothesis; numerical calculations illustrating this support are shown in Fig. 2. Assuming the hypothesis is correct, one can test the statistical theory quantitatively by replacing an average over samples by an average over values of the conductance versus field or energy in a given sample. In particular, it should be possible to extract a sample conductance correlation function which may be compared to the conductance correlation function obtained by ensemble averaging in the next section. It is this notion that we refer to as an "ergodic hypothesis;" a similar hypothesis and terminology is used in the statistical theory of the nucleus.

II. CONDUCTANCE FLUCTUATIONS AT ZERO TEMPERATURE

A. General remarks

In this section we review and extend the zero-temperature theory of the metallic conductance fluctuations. In the first three sections we define and calculate the important statistical quantity, the conductance correlation functions in magnetic field and energy. This section is a more detailed exposition of the results of Ref. 13, including quantitative results on the magnetic field corre-

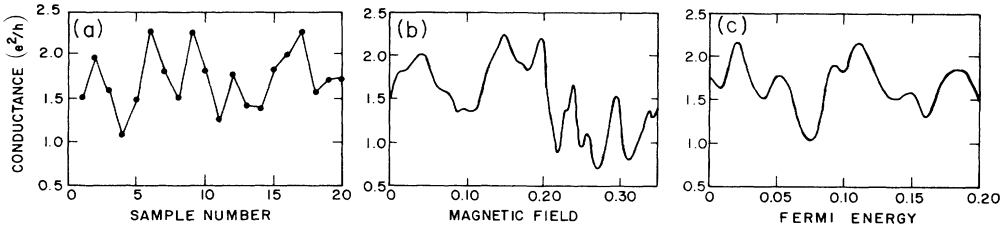

FIG. 2. Comparison of sample-to-sample fluctuations and fluctuations in $g(B)$ and $g(E)$ in a single sample. Data are from numerical simulations on a 100×10 site Anderson model with disorder $W=1$ in units of the hopping matrix element, using the technique of Ref. 11. (a) g for 20 samples differing only in their impurity configurations. (b) $g(B)$ over a range of approximately 10 times the field correlation range. (c) $g(E)$ over a range of approximately 10 times the energy correlation range. Note that the size of the fluctuations is roughly the same in all three cases, lending qualitative support for our ergodic hypothesis; some quantitative support was reported in Fig. 2 of Ref. 13.

lation function, and a discussion of some special properties of this object. In the second part we discuss the appropriate way to introduce inelastic scattering into the calculation, which involves a somewhat subtle physical point, and then assess the corrections to the universal value of the conductance fluctuations introduced by electron-electron interactions. Interestingly, we find that, unlike the case for the average conductance, to lowest order in $(k_F l)^{-1}$ interaction effects can all be included as a contribution to the inelastic scattering rate, and thus do not change the expected physical behavior in an important way.

Before we express the problem in terms of Green functions and Feynman diagrams, we begin by motivating our approach with an analysis in terms of the exact eigenstates of the random system. It has been recognized for some time that in order for the diffusion equation to be satisfied in quantum systems at zero temperature there must be some spatial correlation between the various electron wave functions for each realization of the random potential.[48] This correlation plays a crucial role in enhancing the effect of electron-electron interactions on the average properties of disordered systems. Here, we briefly review the key concepts.

Consider the problem of noninteracting electrons in a random potential. If the randomness is sufficiently weak ($k_F l > 1$, where k_F is the Fermi momentum and l is the elastic mean free path) then the wave functions are extended (in one and two dimensions we assume the localization length is much longer than the sample dimensions). Using the notation of Eq. (1.4), we denote the exact eigenstates for a given impurity configuration as ψ_α and their energies by E_α. The conductivity of such a metallic system will be finite and density fluctuations will relax diffusively. By writing the density-density response function in terms of the exact eigenstates, it was found that the quantity

$$C(E,E',r,r')=\sum_{\alpha,\beta}\langle\psi_\alpha^*(\underline{r})\psi_\beta(\underline{r}')\psi_\beta^*(\underline{r})\psi_\alpha(\underline{r}') \times\delta(E-E_\alpha)\delta(E'-E_\beta)\rangle\ , \quad (2.1)$$

where the angular brackets denote the ensemble average over impurity configurations, is determined by

$$\int dr\int dr'\,C(E,E',r,r')e^{iq\cdot(r-r')}=\frac{dn}{d\mu}\frac{Dq^2}{(E-E')^2+(Dq^2)^2} \quad (2.2)$$

where $D=l^2/d\tau$, is the d-dimensional elastic diffusion constant. Hence the spatial Fourier transform of C is singular for small $\underline{q}$ and $E-E'$, indicating that if $E_\alpha-E_\beta$ is small, then the wave functions ψ_α,ψ_β are also correlated in space. Note that according to Eq. (1.4) the conductance g is an integral over the product of four wave functions. To calculate the magnitude of the conductance fluctuations, given by

$$\langle(g-\langle g\rangle)^2\rangle=\mathrm{Var}(g)\ ,$$

we are thus required to impurity average the product of eight wave functions. A singular behavior arising from wave-function correlation similar to that in Eq. (2.2) thus comes into play, leading to a singular enhancement of the conductance fluctuations. While it should be possible to pursue the calculation further using the exact eigenstate method, and factorizing the product of eight wave functions into the product of two C functions, we find it more convenient to express Eq. (1.4) in terms of Green functions and perform the calculation using more conventional diagrammatic techniques.

The impurity-averaged perturbation theory we will employ is a technique for calculating ensemble averages of various quantities of interest. The theory can be formulated as a systematic expansion in the small quantity (for a metal) $(k_F l)^{-1}$.[56] Our ergodic hypothesis implies that the $\mathrm{rms}(g)=[\mathrm{Var}(g)]^{1/2}$ is a good measure of the typical amplitude of the fluctuations in the conductance versus energy or magnetic field in a single sample, so we certainly want to calculate the statistical variance of g. However, we also would like to know the typical spacing of the peaks and valleys in conductance, i.e., how much the field or energy must be changed in order to change the conductance substantially. This information can also be obtained by ensemble averaging, if our ergodic hypothesis holds. The idea is to define a conductance correlation function

$$F(\Delta E,\Delta B,B)=\langle \delta g(E_F,B)\delta g(E_F+\Delta E,B+\Delta B)\rangle \ , \quad (2.3)$$

where the angular brackets denote the *ensemble* average, and $\delta g = g(E_F,B)-\langle g(E_F,B)\rangle$. The value of this function when $\Delta E=\Delta B=0$ gives the variance (typical size) and the decay lengths in ΔE and ΔB give the energy and field correlation ranges (typical spacing) discussed heuristically in the preceding section. Using the expression for g given in Eq. (1.4), we can express F in terms of Green functions and hence in a form suitable for diagrammatic evaluation using the impurity-averaged perturbation theory mentioned above.

To do this we use the identity

$$\rho(r,r',E)=\langle r \mid (G^+-G^- \mid r'\rangle = -2\pi i \sum_\alpha \psi_\alpha^*(r)\psi_\alpha(r')\delta(E-E_\alpha) \ , \quad (2.4)$$

where $G^\pm=(E-H\pm i\epsilon)^{-1}$. Using Eq. (2.4) to replace the exact eigenstates in Eq. (1.4), we obtain

$$g(E_F)=(1/m^2L_z^2)\int dr \int dr' \left[-\frac{1}{2}\frac{\partial}{\partial z}\frac{\partial}{\partial z'}\rho(r,r',E_F)\rho(r',r,E_F)+\frac{1}{4}\frac{\partial}{\partial z}\rho(r,r',E_F)\frac{\partial}{\partial z'}\rho(r',r,E_F) + \frac{1}{4}\frac{\partial}{\partial z'}\rho(r,r',E_F)\frac{\partial}{\partial z}\rho(r',r,E_F)\right] . \quad (2.5)$$

A diagrammatic representation of a general contribution to $g(E_F)$ before averaging is given in Fig. 3. In this diagram a solid line directed from r to r' represents $G^\pm(r,r')$, the exact (unaveraged) Green function of the noninteracting disordered system, and the crosses represent scattering by impurities located at r_1,r_n. We treat the impurity potential by Born approximation, and assume that the scattering potential from a single impurity is a δ function with strength u^2 (hence isotropic), so that the elastic scattering time is given by $\tau^{-1}=2\pi N_0 c_i u^2$ (N_0 is the density of states of electronic states at the Fermi level, and c_i is the concentration of impurities). Note that since g is bilinear in ρ, the solid lines in the diagram can be either G^+ or G^- in all possible combinations. If we do not ensemble average g is still a function of all the impurity locations, and no further analytic progress can be made, but Eq. (2.4) can be evaluated numerically to find the conductance for that particular impurity configuration.[57,11] The impurity-averaged conductance is a standard calculation;[58] the prescription is to pair up the impurity vertices in all possible ways leading to an effective electron-electron "interaction" mediated by scattering from the same impurity. The simplest self-energy diagrams give a lifetime τ to the average one-particle Green function in momentum representation,

$$\langle G^\pm(p)\rangle = \frac{1}{\zeta \pm i/(2\tau)} \ , \quad (2.6)$$

where $\zeta=\epsilon_p-\mu=p^2/m-\mu$ (henceforward we omit angular brackets and simply denote the average Green function by $G^\pm$). It is then clear that the only nonvanishing contributions to $\langle g\rangle$ are when the two Green functions are of opposite sign G^+G^-. Evaluation of Eq. (2.5) yields the standard Boltzmann result for the conductivity, combined with Ohm's law relating conductivity to conductance,

$$\langle g\rangle = \frac{4\pi N_0 DA}{L_z} \ , \quad (2.7)$$

where A is the cross-sectional area.

B. Variance of g and correlation function in energy

We now turn to the evaluation of Eq. (2.3) for the correlation function F. For simplicity we first consider the case $\Delta B=0$. The diagrams for $\langle \delta g(E)\delta g(E+\Delta E)\rangle$ may be represented schematically as in Fig. 4, which merely represents the product of two conductivity bubbles of the type shown in Fig. 3. Since the correlation function is defined to subtract out the square of the average conductance, upon impurity averaging the only diagrams which contribute to F are those in which impurity lines

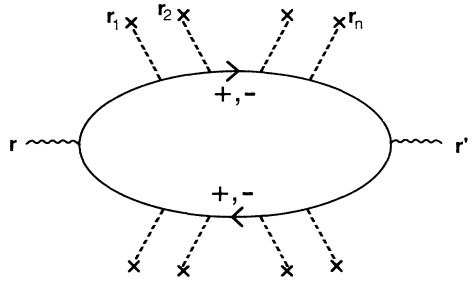

FIG. 3. Diagram for the conductance of a sample *before* impurity averaging. The impurities are represented by crosses. The external field creates a particle-hole pair which propagates from $\vec{r}$ to $\vec{r}\,'$ and the electron line is scattered by impurities located at $\vec{r}_1,\vec{r}_2,\ldots,\vec{r}_n$.

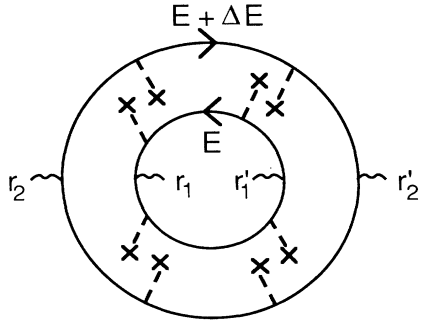

FIG. 4. Diagram for $\langle \delta g(E)\delta(E+\Delta E)\rangle$ before impurity averaging.

connect the two bubbles. The most important diagrams are those where the impurity lines do not cross, since it is well known that such crossings reduce the contribution of a diagram by at least $(k_F l)^{-1}$, by introducing restrictions on the region of integration where the integrand is large. The collection of all such diagrams is shown in Fig. 5. Another set of diagrams in which the particle-hole ladders (diffusons) are replaced by particle-particle ladders (cooperons) is also possible, and in the presence of only normal impurity scattering gives exactly the same contribution as the diagrams shown. The diagrams shown are generated systematically by starting with two concentric loops connected by impurity ladders and inserting the two current vertices on each loop in all possible ways. In Ref. 13, it was erroneously stated that diagrams of the type shown in Fig. 5(d) are cancelled by those of the type shown in Fig. 5(e). This statement is incorrect, two-diffuson diagrams of the type shown in Figs. 5(d) and 5(e) considered alone do give a finite contribution; however, it can be shown that diagrams of this type with two diffusons cancel diagrams of the same type with three diffusons for $\Delta E=0$, so that the final answer is not changed in this case. These diagrams do apparently introduce a very small correction for ΔE not equal to zero, but this is not large enough to affect the comparison with numerical calculations shown in Ref. 13. Further details of this aspect of the diagrammatic calculation will be given elsewhere.[58] Note also that in Ref. 12 (in which only the case $\Delta E=0$ was considered) only the diagrams of Fig. 5(a) were kept and evaluated; hence the results given there are incomplete and the numerical value obtained for $F(0)=\mathrm{Var}(g)$ is incorrect. However, it is found after evaluating all the diagrams that the behavior of $\mathrm{Var}(g)$ is qualitatively the same as that obtained by only evaluating Fig. 5(a) (i.e., size and disorder independent).

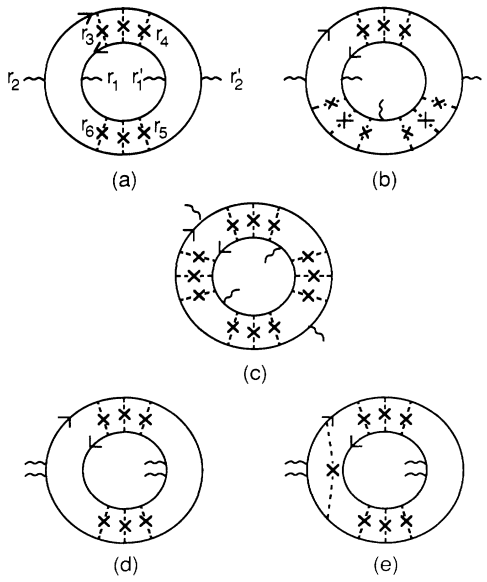

FIG. 5. Diagrams which contribute to the impurity averaged $\langle \delta g(E)\delta g(E+\Delta E)\rangle$.

The feature which makes the diagrams shown in Fig. 5 the dominant contribution to F is the singular behavior at small momentum and frequency associated with the impurity ladder connecting two Green-function lines with opposite analyticity, G^+ and G^-. When arrows on the Green-function lines are opposite, as in Fig. 6(a), the diagram represents particle-hole excitation, i.e., density fluctuations, and is proportional to the characteristic diffusion pole $[\tau(Dq^2-i\Delta E)]^{-1}$. The diagrams shown in Fig. 5 are the only ones where the diffusion poles all occur with the same momentum transfer q. We shall refer to Fig. 6(a) as the particle-hole channel. It should be noted that Fig. 6(a) denotes the diffusion ladder at zero frequency (which would come into the dc conductance) but evaluated at different values of the Fermi energy; hence the energy difference which comes into the correlation function for the dc conductance plays exactly the same role formally as a finite frequency but with a very different physical significance. When the arrows in the diffusion ladder are parallel, as in Fig. 6(b), we have the particle-particle channel. Provided that time-reversal symmetry is not broken, the diagrams in Fig. 6(a) and 6(b) give equal contributions.

To see the general structure of the divergences in this theory we consider the diagram shown in Fig. 5(a), evaluated for the infinite system, where it is permissible to work in momentum space. There are two diffusion poles associated with the two impurity ladders, and both poles occur with the same $\underline{q}$ and ΔE. Setting $\Delta E=0$ and integrating over $\underline{q}$, we see that this diagram is infrared divergent below four dimensions. This divergence is cut off at finite size by the sample dimensions which determine a cutoff momentum $q_c \sim L^{-1}$, so that such diagrams are enhanced by the divergent behavior by a factor L^{4-d}. This infrared divergence is the reason that the conductance fluctuations do not decrease with size as they would for a classical resistor network. In the Introduction we argued that classical resistor networks have central-limit-type scaling behavior: $\mathrm{Var}(g)/\langle g\rangle^2 \sim L^{-d}$, leading to Eq. (1.7), $\mathrm{Var}(g)\sim L^{d-4}$, for the *classically expected* behavior of the absolute variance of the conductance. The L^{4-d} enhancement arising from the divergences associated with

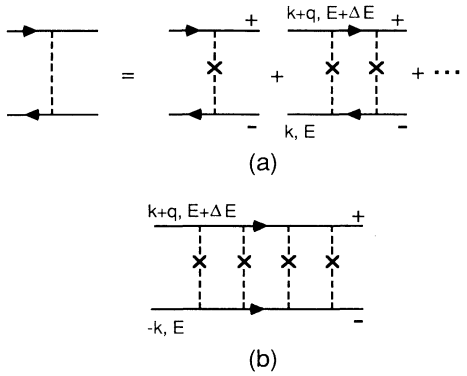

FIG. 6. (a) Particle-hole ladder; (b) particle-particle ladder.

quantum diffusion exactly cancel this classical self-averaging behavior, leading to the result that $\mathrm{Var}(g)=F(\Delta E=0)$ is simply a number of order unity, independent of size.

We note that divergences of this kind in the second moments of physical quantities calculated by impurity-averaged perturbation theory were first treated in a paper by Maldague.[59] However, he evaluated the density response (as opposed to the current response as we do here) and a number of diagrams where a single impurity line crosses the density vertex were omitted. These diagrams typically would cancel the leading singularities, so that without a careful reevaluation of all the diagrams it is not clear whether the divergences discussed by Maldague are real.

In order to evaluate F quantitatively to obtain the absolute magnitude of the conductance fluctuations we must evaluate Eq. (2.3) for a finite sample, thus the diagrams must be formulated in real space. The details of this less-common formulation are given in Appendix A. As is shown in Appendix A, the final result is obtained by summing the diagrams shown in Figs. 5(a), 5(b), and 5(c) for both the particle-hole and particle-particle channel; for the case $B=\Delta B=0$, and no spin-orbit or spin-flip scattering, we find

$$F(\Delta E)=2\left[\frac{4}{\pi^2}\right]^2(F_1+F_2+F_3)\ , \tag{2.8}$$

where

$$F_1=2\sum_{m_x,m_y=0}^{\infty}\sum_{m_z=1,3,5,\ldots}[\mathrm{Re}(\tilde{\lambda}_m^{-1})]^2\ , \tag{2.9a}$$

$$F_2=-8\,\mathrm{Re}\left[\sum_{m_x,m_y=0}^{\infty}\sum_{m_z=1,3,5,\ldots}{}'\sum_{n_z=2,4,6,\ldots}{}'\frac{(f_{mn})^2}{\tilde{\lambda}_m\tilde{\lambda}_n}\left[\frac{1}{\tilde{\lambda}_m}+\frac{1}{\tilde{\lambda}_n}\right]\right]\ , \tag{2.9b}$$

$$F_3=24\,\mathrm{Re}\left[\sum_{m_x,m_y=0}^{\infty}\sum_{m_z,p_z=1,3,5,\ldots}{}'\sum_{n_z,q_z=2,4,6,\ldots}{}'\frac{f_{mn}f_{np}f_{pq}f_{qm}}{\tilde{\lambda}_m\tilde{\lambda}_n\tilde{\lambda}_p\tilde{\lambda}_q}\right]\ , \tag{2.9c}$$

where $f_{mn}=4m_zn_z/\pi(m_z^2-n_z^2)$ and the primes denote sums over even or odd integers only. As discussed in Appendix A, the quantities $\tilde{\lambda}$ appearing in the above equations are the (scaled) eigenvalues of the diffusion equation

$$\tau(-i\,\Delta E+D(-i\,\vec{\nabla})^2+\tau_{\mathrm{in}}^{-1})Q_m(\underline{r})=\lambda_vQ_m(\underline{r})\ , \tag{2.10}$$

where this diffusion equation is to be solved with the boundary conditions $Q_m=0$ at the boundary with the perfect leads, and $(\vec{\nabla})\cdot\hat{n}Q_m=0$, where $\hat{n}$ is the unit normal at the vacuum interface. For a rectangular sample the eigenvectors are simply

$$Q_m(\underline{r})=(8/L_zL_xL_y)^{1/2}\sin(m_z\pi z/L_z)\times\cos(m_x\pi x/L_x)\cos(m_y\pi y/L_y)\ ,$$

where $m_z=1,2,\ldots,\infty$, $m_{x,y}=0,1,2,\ldots,\infty$, and the eigenvalues are $\lambda=D(\pi/L_z)^2\tilde{\lambda}_m$,

$$\tilde{\lambda}_m=m_z^2+m_x^2(L_z^2/L_x^2)+m_y^2(L_z^2/L_y^2)+\gamma-i\eta\ , \tag{2.11}$$

and $\gamma=(L_z/\pi L_{\mathrm{in}})^2$, where $L_{\mathrm{in}}=(D\tau_{\mathrm{in}})^{1/2}$ is the inelastic diffusion length, and $\eta=\Delta E\,L_z^2/(\hbar\pi^2D)$. Note that Eqs. (2.8) and (2.9) confirm our initial assumption that the correlation function is only a function of the energy difference, ΔE, and not of E_F.

First, the evaluation of Eqs. (2.9) and (2.10) for $\Delta E=0$ ($\eta=0$) and $L_{\mathrm{in}}^{-1}=\gamma=0$, gives us rms($g$), the typical size of the fluctuations at zero temperature. We note again that the size of the conductor has totally cancelled out, leaving only factors relating to its shape. In addition, the shape dependence is very weak, as can be seen by noting that the lowest eigenvalue $\tilde{\lambda}(m_z=1,m_x=m_y=0)$ dominates the sums in Eq. (2.9) as long as $L_z\geq L_x,L_y$. This may be traced back directly to the boundary condition that current only flows in the z direction. The sums appearing in Eq. (2.9) can be evaluated numerically with high accuracy since they converge rapidly, and we find for a quasi-1D sample rms(g)=0.729, for a 2D square rms(g)=0.862, and for a 3D cube rms(g)=1.088. These values are reduced by spin-flip and spin-orbit scattering in a manner which is calculated in Appendix C. Equation (2.9) implies that the shape-dependence of rms(g) *does* become strong when either L_x or L_y are longer than L_z, then rms(g)$\sim(L_xL_y)^{1/2}/L_z$, and it is possible to obtain values for the rms(g) much greater than e^2/h. The same shape-dependent enhancement can occur at finite temperature also (see the discussion at the end of Sec. III C).

The second result rigorously obtained from Eq. (2.9) is the energy correlation range, E_c, which is the typical scale of the *spacing* between peaks and valleys in g as a function of E_F. According to our ergodic hypothesis, as discussed earlier, E_c is simply the half-width of $F(\Delta E)$. This is approximately determined by the condition $\eta=1$, i.e., $E_c\simeq\hbar\pi^2D/L_z^2$, which, as noted in the Introduction, is just the inverse time for the particle to diffuse across the sample in the current direction. Various physical arguments for the appearance of this quantity in this context were given in the Introduction, and elsewhere.[46,55] In Ref. 13 it was shown that the analytic results for $F(\Delta E)$ given here agree with numerical calculations to an accuracy of about 5% without any free parameters.

Third, it is interesting to note that $F(\Delta E)$ decays very slowly as a function of $\Delta E/E_c$ and shows a nontrivial dependence on dimensionality. Asymptotic evaluation of Eq. (2.9) yields

$$F(\Delta E)\sim(E_c/\Delta E)^{(4-d)/2}\ . \tag{2.12}$$

This is very different from the exponential decay of correlations exhibited by normal Poisson processes and indicates a kind of long-range memory in the fluctuations of $g(E_F)$. In fact, this decay is so slow in three dimensions that energy-averaging arguments based on the assumption, that values of the conductance separated by more than E_c are essentially uncorrelated, fail in three dimensions, leading to an anomalously slow temperature dependence of rms(g) (see Sec. III).

C. Correlation function in magnetic field

Now we turn to the evaluation of the magnetic field correlation function, $F(\Delta B,B,\Delta E=0)$ at $T=0$. This quantity is also given by the sum of the diagrams in Figs. 5(a), 5(b), and 5(c), now evaluated at finite B and ΔB. The magnetic field enters the calculation by means of the usual semiclassical approximation for the Green function, appropriate when the cyclotron radius is much greater than the elastic mean free path,[60]

$$G(r,r',B)=\exp\left[(2\pi i/\phi_0)\int_{r'}^{r} A\cdot ds\right]G(r-r') ,$$

where $\phi_0=h/e$, $G(r,r')$ is the average Green function in the absence of the field, and the line integral is evaluated along the straight line between r and r'. Since it is the product $G(r,r')G(r',r)$ which comes into the particle-hole channel, only the vector potential difference ΔA will appear in the particle-particle contribution to F; it appears in the diffusion equation in the usual way, so $F_{\rm ph}$ is determined by the eigenvectors and eigenvalues of

$$\tau(-i\,\Delta E+D(-i\vec{\nabla}-e\,\Delta A)^2+\tau_{\rm in}^{-1})Q_m(\underline{r})=\lambda_\nu^{\rm ph}Q_m(\underline{r}) . \tag{2.13}$$

Whereas for the particle-particle channel it is essentially $G(r,r')^2$ which appears, leading to a diffusion equation determining $F_{\rm pp}$ of the form

$$\tau(-i\,\Delta E+D(-i\vec{\nabla}-e(2A+\Delta A))^2+\tau_{\rm in}^{-1})Q_m(\underline{r}) =\lambda_\nu^{\rm pp}Q_m(\underline{r}) . \tag{2.14}$$

When $B=\Delta B=0$, the particle-hole and particle-particle channels give equal contributions to F, leading to the overall factor of 2 in Eq. (2.8); when B is nonzero the two contributions must be evaluated separately from Eqs. (2.13) and (2.14). The first diagram F_1 can be evaluated as before with the eigenvalues $\tilde{\lambda}$ replaced by $\tilde{\lambda}^{\rm ph}(\Delta B)$ and $\tilde{\lambda}^{\rm pp}(2B+\Delta B)$, respectively. However, F_2 and F_3 involve matrix elements of the eigenfunctions of the relevant diffusion equation which have to be evaluated as discussed in the Appendix A, and which will no longer simply give the factors f_{mn} which appear in Eqs. (2.9b) and (2.9c). Therefore a precise quantitative evaluation of all three diagrams in both channels for nonzero B and ΔB requires solution of Eqs. (2.13) and (2.14) on a finite system with the mixed boundary conditions discussed in Appendix A. Although straightforward in principle, we do not attempt such a solution here, but only evaluate properties of F in various limits.

First we note that because the contribution from the particle-particle channel depends on the value of the field as well as the field difference, the full correlation function is in general a function of B and ΔB. However, once $BL_zL_x\gg\phi_0$ (where L_zL_x is the sample area normal to the field) the solutions of Eq. (2.14) are simply Landau levels (in two dimensions) with uniformly spaced eigenvalues,

$$\tilde{\lambda}_n^{\rm pp}=(n+\tfrac{1}{2})(4/\pi)[(2B+\Delta B)L_z^2]/\phi_0 .$$

Hence the lowest eigenvalue will be much greater than one, whereas the lowest eigenvalue will still be order unity in (2.13), and since the inverse of the lowest eigenvalue in

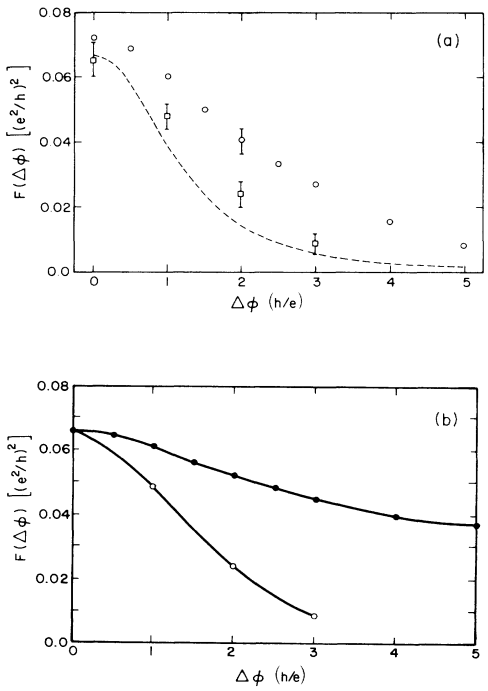

FIG. 7. (a) Comparison of analytic and numerical solutions for the correlation function in magnetic field. Dashed line is the analytic solution for the 1D magnetic field correlation function calculated using the perturbative solution to Eq. (2.13) described in the text. Changes in field are measured in terms of the flux normal to the wire in units of h/e, $F(\Delta\phi)$ is measured in units of $(e^2/h)^2$. The particle-particle contribution is assumed to be totally suppressed. Squares are the result of numerical calculations for a 400×40 site Anderson model with $W=1$, $E=0.2$, in units of the hopping matrix elements. Circles are numerical results for a 200×20 site system with otherwise the same parameters. Comparison is made with no free parameters. Clearly the numerical solutions show better agreement for the larger sample size, suggesting that there are some finite-size corrections to the numerical results as discussed in the text. In the numerical calculations the initial value of the field corresponded to 20 flux quanta in the former case and 10 flux quanta in the latter. This was chosen to suppress the particle-particle contribution as discussed in the text. (b) Comparison of field correlation ranges obtained numerically for a 20×20 square with $W=4$ (solid circles) and a 400×40 strip with $W=1$ (open circles). $F(0)$ for the 2D case has been normalized to the 1D value for comparison.

each channel determines the order of magnitude of its contribution, the contribution from the particle-particle channel will be negligible for $BL_zL_x \gg \phi_0$. It is for essentially the same reason that the weak localization effects in the average conductance saturate for large magnetic fields. Thus when the flux through the sample is much greater than h/e, $F(B,\Delta B) \simeq F_{\rm ph}(\Delta B)$, and $F(B,0) \simeq F_{\rm ph}(B,0) = \frac{1}{2}F(0,0)$, and simply dividing our above results for Var(g) by two gives the expected rms value of the aperiodic magnetoconductance fluctuations, δg_B,

$$\delta g_B = \begin{cases} 0.52, & d=1 \\ 0.61, & d=2 \\ 0.78, & d=3 \, . \end{cases} \tag{2.15}$$

There is one caveat to the above analysis that will be explained below in the section discussing the symmetry of $g(B)$.

From this point on we will assume that the magnetic field is large enough that the particle-particle channel is negligible and then consider the correlation function $F_{\rm ph}(\Delta B)$ with the appropriate factor of $\frac{1}{2}$ reduction of its amplitude (we will now suppress the label ph). One important consequence immediately follows from the fact that only the field *difference* now appears in F. The aperiodic magnetoresistance fluctuations should persist in field at least until the cyclotron radius becomes smaller than l, since this is the condition for the validity of the semiclassical approximation used above. This corresponds to a very high field in a typical metal and explains one of the most surprising features of the experiments, the persistence of the fluctuations unchanged to fields as high as 16 T. This behavior is to be contrasted with the well-known weak localization corrections to the average conductance, which come entirely from quantum interference in the particle-particle channel, and which therefore die off rapidly when a flux of order h/e penetrates the sample area (or an area of size $L_{\rm in}^2$ at finite temperature). The fact that the essential behavior of the conductance fluctuations can be obtained by considering only the particle-particle channel makes clear formally the physical point made in the Introduction: The fluctuations effects we calculate are not localization effects in any obvious sense.

We can obtain the eigenvalues needed to evaluate $F(\Delta B)$ most easily in two limits. First, for small ΔB the field difference only gives a perturbative correction to the eigenvalues obtained from Eq. (2.10). This perturbative correction is, however, sufficient to allow us to estimate the correlation range in magnetic field, which determines the typical spacing of the fluctuations in magnetic field in a given sample. Hence we must solve Eq. (2.13) perturbatively with (choosing a gauge) $\Delta \vec{A} = \Delta B x \hat{z}$. Since our general solution for F is dominated by the lowest eigenvalues, the correlation field may be obtained simply from perturbation theory for these lowest eigenvalues. From Eq. (2.13) we see that the perturbation has the form $V' = V_1' + V_2'$, where

$$V_1' = -2ie\,\Delta B\, x \frac{d}{dz}$$

and $V_2' = (e\,\Delta B\, x)^2$. We denote the unperturbed eigenstates defined above by $\langle m_z m_x m_y |$, the perturbed eigenvalues can still be labeled as $\tilde{\lambda}_{m_z m_x m_y}$. For consistency we need to calculate corrections to second order in V_1', and first order in V_2'. The calculation simplifes considerably for the quasi-one-dimensional case ($L_z \gg L_x, L_y$). L_y, the direction parallel to the field is irrelevant to this discussion, and henceforward indices related to this direction will be suppressed. V_1' has no diagonal matrix elements by symmetry, and the diagonal element of V_2' for the states $\langle m_z, 0 |$ just gives

$$\tilde{\lambda}_{m_z 0}(\Delta B) \simeq m_z^2 + 1/3(\Delta B\, L_x L_z/\phi_0)^2 \, . \tag{2.16}$$

In addition, off-diagonal elements of V_1' of the form $\langle m_z 0 | V_1' | m_z' 0 \rangle$ vanish, as do all off-diagonal elements of V_2'. Therefore it follows simply from the form of the unperturbed eigenvalues that Eq. (2.14) is the correct perturbative expression for the lowest eigenvalues up to corrections of order $(L_x/L_z)^2(\Delta B)^2$, which are negligible for this quasi-one-dimensional geometry. Equation (2.14) is then a good approximation until the field-dependent correction is of the order of the spacing of the eigenvalues with different values of m_x, which yields the condition $(\Delta B\, L_z L_x/\phi_0)^2 \sim (L_z/L_x)^2$, i.e., $\Delta B\, L_x^2 > \phi_0$. To estimate the $T=0$ correlation field we can set this correction equal to the lowest unperturbed eigenvalue; B_c is then determined by the condition $\delta\tilde{\lambda}(\Delta B = B_c) \simeq 1$, which gives the result $B_c \simeq \sqrt{3}\phi_0/L_zL_x$ where L_zL_x is the sample area normal to the field. A full evaluation of the diagrams using this 1D perturbative correction to the eigenvalues yields a more precise value of $B_c \simeq (1.2)\phi_0/L_zL_x$. In Fig. 7(a) we show a comparison with no free parameters between the analytically calculated correlation function $F(\Delta B)$ in this approximation and the numerically calculated correlation function evaluated for two different size quasi-1D samples of the same shape. Note that agreement on the value of B_c is much better for the larger sample, suggesting that finite-size effects affect this quantity much more than the amplitude of the correlation function. In particular, the diffusion equation for $\lambda(\Delta B)$ is only correct when the sample dimensions are much larger than the elastic mean free path, which is not the case for the degree of disorder and sample sizes which may be explored numerically in a quasi-1D geometry without making the sample shorter than the localization length. In two dimensions this is not a problem, and no similar sensitivity of B_c to sample size is observed numerically; hence this finite-size effect is probably the origin of the small discrepancy shown in Fig. 7(a). This problem with the numerical simulations of $F(\Delta B)$ was not appreciated in Ref. 13, where an incorrect value $\phi_c \simeq 2.4\phi_0$ was given.

As the sample aspect ratio is changed from a long strip to a square, the second-order contribution in V_1' from states with m_x not equal to zero increases in magnitude, and the contribution to the lowest eigenvalue is always negative. This means that the coefficient of the ΔB^2 term in Eq. (2.16) decreases with decreasing aspect ratio, $s = (L_z/L_x)^2$, and thus the field correlation range gets longer. This trends is illustrated in the numerical calculations of $F(\Delta B)$ shown in Fig. 7(b). The magnitude and shape-dependence of B_c clearly should have an interpreta-

tion in terms of the rms area enclosed by two random walks across the sample for a given shape of the diffusion region, as discussed in our Introduction.

Finally, the magnetic field correlation function also exhibits a slow, dimension-dependent power-law decay, asymptotically

$$F(\Delta B)\sim\left[\frac{B_c}{\Delta B}\right]^{4-d}. \tag{2.17}$$

As before, at $T=0$ the relevant dimensionality is determined by the shape of the sample, except that for a long thin strip ($L_z \gg L_x$) the decay will still become two dimensional asymptotically when $(\Delta B\, L_x L_z/\phi_0) > (L_z/L_x)$.

We now present a final point relating to the amplitude of the fluctuations in $g(B)$. It is well known that $\langle g(B)\rangle$ exhibits negative magnetoresistance for small magnetic fields due to weak localization effects[55] (for the case of normal impurity scattering). This effect has been seen experimentally in good agreement with the theory[51] for relatively large samples. Therefore the question arises whether this average behavior of $g(B)$ will be visible in typical small samples at low temperatures, or whether it will be masked by the fluctuations of order e^2/h. In one and two dimensions the maximum amplitude of the average effect is determined by the inelastic diffusion length (when that length is shorter than the sample dimensions), but it is easy to show that for a finite system the maximum amplitude of the average conductance rise at $T=0$ is of order e^2/h, in one dimension, and of order $(e^2/h)\ln(L_B/l)$ in two dimensions (where $L_B^{-2}=2eB/\hbar c$). Therefore the size of the two effects should be comparable in one and two dimensions and numerical calculations on 2D wires indicate that the fluctuation effects can be somewhat larger; this is illustrated in Fig. 8, where the average behavior is contrasted with the behavior of a single sample. Thus we do not expect small MOSFET's at low T to show a clear weak-localization negative magnetoresistance. For small metal wires and films the situation is a bit more complicated, since the amplitude of the 3D negative magnetoresistance can be much larger than e^2/h. This raises issues of dimensional crossover which we have analyzed and which indicate that the relative size of the average and fluctuation effects in $g(B)$ depends in detail on the sample parameters, and no general statement can be made about which effect will dominate. Details of this analysis will be presented elsewhere.[46]

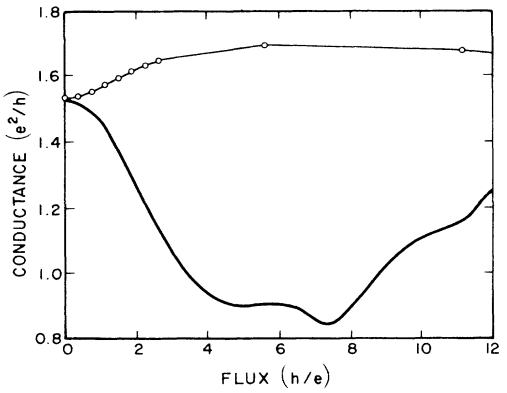

FIG. 8. Comparison of average weak localization positive magnetoconductance (open circles) and typical behavior of a single sample (solid line). Numerical calculations for a 100×10 strip with $W=1$, average was taken over 1000 samples. $g(B=0)$ for single sample is normalized to $\langle g(B=0)\rangle$.

D. Symmetry of $g(B)$

As noted above, there is one case in which the contribution of the particle-particle channel to the correlation function is not negligible, even at large absolute values of the magnetic field. That arises when one considers the correlation of $g(B)$ and $g(-B)$. The factor $2B+\Delta B$ which comes into the diffusion equation for the particle-particle channel is actually the sum of the fields on the inner and outer loops. Hence if one considers $F(B, \Delta B=-2B)$, the particle-particle contribution will be independent of the absolute value of B, and will give as large a contribution as the particle-hole channel. It is easy to check that this result is required to insure that $\langle[g(B)-g(-B)]^2\rangle=0$, i.e., that $g(B)$ as we have defined it above is symmetric around $B=0$.[14] This result is guaranteed to hold in our theory by time-reversal symmetry and the relation $g=\mathrm{Tr}(t^\dagger t)$. Here the detailed form of the multichannel Landauer formula used is important. For a more complicated formula such as that of Refs. 33 and 34 time-reversal symmetry does not imply that $g(B)=g(-B)$, and indeed evaluation of $g(B)$ using that formula does yield an asymmetry.[61,11] Some experiments have also observed a substantial asymmetry,[1] which is in fact much larger than that obtained in simulations of the formula used in Ref. 61, but whose origin is still not completely clear. Any frozen magnetic field in the material which does not reverse exactly with the external field can of course give rise to an asymmetry, and it has recently been suggested that a small number of frozen magnetic moments may be the explanation of the experimental effect.[62] The natural suggestion that spin-flip scattering from magnetic impurities could be the source of the asymmetry by preferentially damping the Cooperon channel turns out to be incorrect for this problem, as is discussed briefly in Appendix C.

A different explanation of the asymmetry is suggested by a natural inference from a result obtained in Ref. 14. In Ref. 14 it was shown that when a current is flowing in the x direction, it induces fluctuations of order e^2/h in the transverse conductance, g_{xy}, *even in the absence of a magnetic field.* It is possible that under certain experimental conditions a voltage measurement between two points separated along the x direction will nonetheless measure some combination of g_{xx} and g_{xy}. Then, if g_{xy} for a given sample has no definite symmetry under reversal of the field one would expect to observe a large apparent asymmetry in the voltage drop at fixed current when the field is reversed. Of course on the average the conductivity σ_{xy} is asymmetric in field and the term proportional to B gives the Hall coefficient. However, recent work by Ma and Lee[63] has shown that in a given sample $\sigma_{xy}(B)$ has no definite symmetry, making possible an ex-

planation of the type suggested above. Another approach, which has been taken very recently by Büttiker,[64] is to derive a four-probe version of the Landauer formula, from which it can be shown that conductance measurements between any two probes need not yield symmetric results under field reversal. This then gives a natural explanation of the experimental asymmetry similar in spirit to that suggested above, although no quantitative estimates of its size have yet been made using this approach. Finally, very recent experiments by Benoit *et al.*[65] seem to indicate that an explanation of essentially this type is correct, since they show that experimentally one can separate out the symmetric and antisymmetric contribution to g by a simple lead-switching procedure.

E. Effects of interaction

The above discussion of the zero-temperature conductance fluctuations has been restricted to the case of noninteracting fermions in a random potential. It is now well known that interaction effects in the presence of disorder have an important effect on the behavior of the *average* conductance both at finite, and at zero temperature. In fact, these may be the dominant effects in certain experimental contexts, so it is necessary to examine the effect of interactions on the universal conductance fluctuations in order to predict the experimental behavior with confidence. In this section we show that at $T=0$ interactions do not effect the numerical value of the universal conductance fluctuations to the leading order in $(k_F l)^{-1}$ which we have been considering; and at finite temperature including interactions simply leads naturally to the introduction of a finite inelastic scattering rate. Another way of stating this second result is that the presence of a τ_{in}^{-1} cutoff in Eq. (2.10), which was put in by hand on physical grounds in Ref. 13, is derived below rigorously for the case of electron-electron scattering.

The crucial point is that in the diagrams which contribute to the fluctuation correlation function F, only static impurity lines are permitted to connect the inner and outer loop. Formally this is because F represents the average of the product of two four-point functions, and not one eight-point function. Physically, this is because each loop represents a separate conductance measurement, and they are correlated only to the extent that the electrons experience the same static impurity potential. This means that no interaction lines can connect the inner and outer loops, thus we need consider only two ways of inserting interaction lines into the basic diagrams.

First, interaction lines may be inserted into the part of the diagrams between the current vertices and the diffusion propagator, as shown in Figs. 9(a) and 9(b). Corrections of the type shown in Fig. 9(a) can clearly be taken into account as a shift of the chemical potential from its value in the noninteracting system. Corrections of the type shown in Fig. 9(b) (with the interaction vertices dressed by diffusons) are analogous to the corrections to the average density of states of disordered metals found previously.[66] These do introduce corrections to the zero-temperature value of the conductance fluctuations, but they are of order $(k_F l)^{-1}$ compared to values calculated above, so in principle the "universal" value of the conductance fluctuations has the form

$$\text{rms}(g)=O(1)+O((k_F l)^{-1}) .$$

It is true that this correction, though down by $(k_F l)^{-1}$, is divergent for $d \leq 2$ as L^{2-d}. However, these corrections are of the same order as weak localization, and we have assumed that we are in a regime where such corrections are small for a typical finite-size sample. Hence the $T=0$ values of the universal conductance fluctuations, and the behavior of the correlation functions, are essentially unchanged by including interaction corrections of the type discussed above.

The second type of interaction corrections we need consider are self-energy type corrections to the diffusion propagator of the sort shown in Figs. 10 and 11. However, such corrections go to zero at $T=0$, and at finite T such diagrams only introduce a cutoff in the diffusion propagator which can be identified as the electron-electron inelastic scattering rate [justifying its presence in Eq. (2.10)]. This may at first seem surprising because the usual diffusive form of the density-density correlation function is a consequence of particle number conservation and is not affected by inelastic scattering. However, we recall that mathematically this conservation law is im-

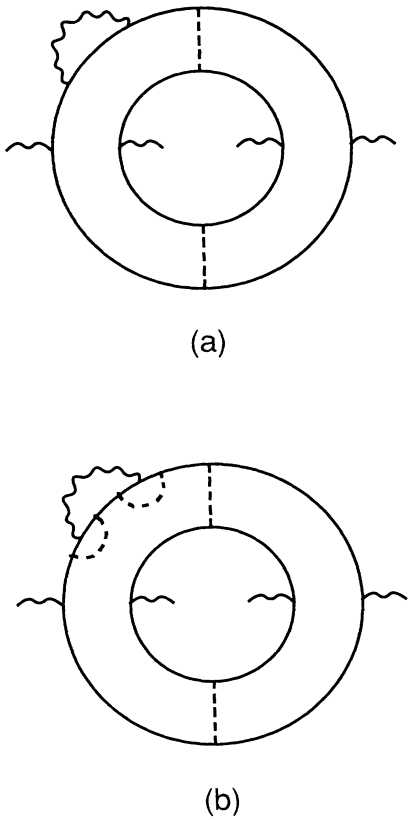

FIG. 9. Interaction corrections to Fig. 5(a) where the interaction (represented by wavy lines) appears between the external vertex and the diffusion propagator.

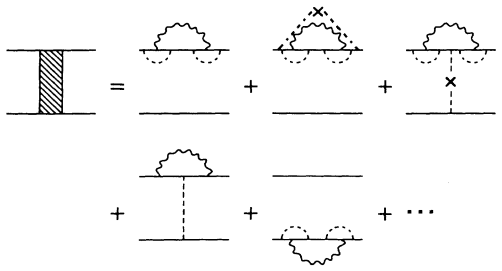

FIG. 10. Self-energy-type correction to the diffusion propagator.

posed by the Ward identity which states that vertex corrections (interaction lines connecting the particle and hole lines in Fig. 10) exactly cancel the self-energy corrections due to interactions. In the present problem, the object we are calculating is not the density-density correlation function, and for the reason mentioned above such vertex corrections are not allowed. The absence of the usual cancellation then leads to the appearance of $\tau_{\rm in}^{-1}$ in Eq. (2.10).

More explicitly, the diagrams leading to the introduction of the cutoff $\tau_{\rm in}^{-1}$ are shown in Figs. 10 and 11. We just note that the calculation of Fig. 10 has been carried out elsewhere for the particle-particle channel.[67] It has also been recognized that the same calculation gives the same result for the particle-hole channel.[68] The end result of including the contributions of Figs. 10 and 11 is then to replace the diffusion pole Dq^2 by $Dq^2+\tau_{\rm in}^{-1}$, where $\tau_{\rm in}^{-1}$ is proportional to $T^{3/2}$ in three dimensions.[69] In one and two dimensions the calculation needs to be done self-consistently, leading to a $\tau_{\rm in}^{-1}$ proportional to T in two dimensions and to $T^{2/3}$ in one dimension, in agreement with the conclusions of Altshuler *et al.*[70]

It is worth contrasting this situation with the effect of inelastic scattering on both the weak-localization effects and the interaction effects in the average conductance. In the interaction effects on the average conductance (and other average properties) at finite temperature kT itself enters as a cutoff to the singularity, and $\tau_{\rm in}^{-1}$ does not appear explicitly, precisely because the interaction effect comes from singular behavior of the density-density correlation function, and the appearance of $\tau_{\rm in}^{-1}$ is forbidden by particle conservation. On the other hand, for the weak localization effects $\tau_{\rm in}^{-1}$ does appear as a cutoff, because

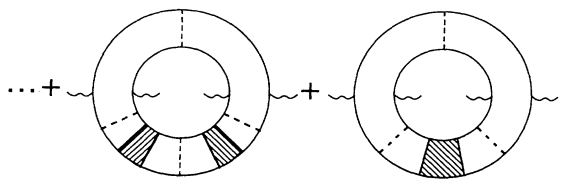

FIG. 11. Corrections of the type given in Fig. 10 inserted in Fig. 5(a). These diagrams lead to the appearance of an inelastic scattering rate as a cutoff.

these arise from singularities in the particle-particle channel, where no exact cancellation of vertex corrections occurs; but kT does not appear as a cutoff. Formally, this is because weak localization occurs for noninteracting particles, and one can always calculate the average conductance in terms of the exact single-particle eigenstates, where it is clear that an average over a finite-temperature Fermi distribution of occupied and unoccupied states does not affect the result. Physically one can argue that the weak-localization coherent backscattering has a fixed phase which is unaffected by energy changes of order kT, as will be discussed in the next section. In the present problem both inelastic scattering and thermal smearing are important at finite temperature, and their effects need to be considered carefully as we do in the next section.

III. CONDUCTANCE FLUCTUATIONS AT FINITE TEMPERATURE

A. General remarks

Having reviewed the calculation of the conductance correlation functions at zero temperature, we now discuss the behavior of the correlation functions at finite temperature. The well-verified picture of quantum transport in metals which comes out of the work of Thouless[71] and the scaling theory of localization is that a metal exhibits purely quantum transport up to the length scale $L_{\rm in}$, the inelastic diffusion length, and classical Boltzmann transport beyond that scale. We expect, therefore, that the fluctuation effects studied above (which are scale independent in the zero-temperature quantum limit, but scale dependent classically) will have a temperature-dependent amplitude once the temperature is high enough that the inelastic length becomes shorter than the sample dimensions. To be more specific, in the Introduction we noted that classically the conductance of a sample depends on the conductances of smaller subregions in an essentially additive way; and this leads to a central limit type of behavior of $\mathrm{Var}(g)$: $\mathrm{Var}(g)/\langle g\rangle^2\sim L^{-d}$, hence $\mathrm{rms}(g)\sim L^{(d-4)/2}$ (since by Ohm's law $\langle g\rangle\sim L^{d-2}$). Thus we expect that the amplitude of the fluctuations should decrease with increasing T (for fixed sample size) once the inelastic length becomes shorter than the sample length as

$$\mathrm{Var}[g(L,T)]\simeq\mathrm{Var}[g(L_{\rm in})](L_{\rm in}/L)^{4-d}\,. \tag{3.1}$$

It turns out that typically in a metal there will also be some weak temperature dependence of $\mathrm{Var}[g(L_{\rm in})]$ due to an effect we refer to as "energy averaging" which will be discussed in detail below. In this section we calculate the detailed temperature dependence in all dimensions of $\mathrm{rms}[g(T)]$, and of the correlation ranges in magnetic field and chemical potential, $B_c(T)$ and $\mu_c(T)$, as well as the criteria for dimensional crossover at finite temperature.

The size dependence of $\mathrm{Var}[g(L,T)]$ indicated by Eq. (3.1) is to be contrasted with the behavior of quantum corrections to the average conductance in two dimensions due to either weak localization or interaction effects whose magnitude is determined solely by a T-dependent length scale (once that scale becomes smaller than the sample dimensions). If one then imagines scaling the

sample at a fixed nonzero temperature, the quantum fluctuation effects described above do vanish as a power of the system size, whereas the quantum corrections to the average conductance are approximately scale independent and persist. Thus even though the fluctuation effects and the average corrections to g can be of comparable magnitude in macroscopic samples at $T=0$, the thermally-induced classical self-averaging will reduce the fluctuations greatly relative to the average effects at experimentally accessible temperatures. This is why these fluctuation effects were not evident in most of the experiments which detected weak localization or interaction effects in quasi-1D or quasi-2D samples (the situation in three dimensions is more complicated, as discussed above). Nonetheless, the result (anticipated above) that the fluctuation effects only decrease as a slow power law of T indicate that such effects should be detectable in rather large samples (or alternatively at rather high T in small samples) if an experiment is designed to look for them.

The simple argument leading to Eq. (3.1) determines correctly $\mathrm{Var}[g(L,T)]$ once $L_{\mathrm{in}}<L$, if one knows $\mathrm{Var}[g(L_{\mathrm{in}},T)]$ the variance of a subregion of size L_{in} at temperature T. The complexity of the analysis of $\mathrm{rms}[g(T)]$ and related quantities which arises below comes about because there exist two T-dependent length scales relevant for the analysis of $\mathrm{rms}(g)$. The first is of course the inelastic diffusion length $L_{\mathrm{in}}=(D\tau_{\mathrm{in}})^{1/2}$, and the second is the thermal length, $L_T=\sqrt{hD/kT}$. *Both* of those length scales come into the analysis of $\mathrm{rms}[g(T)]$, unlike the situation for the weak-localization effects, where only L_{in} is relevant, or the interaction effects, where only L_T is relevant. We find below that if $L_{\mathrm{in}}<L_T$, then $\mathrm{Var}[g(L_{\mathrm{in}},T)]=\mathrm{Var}[g(T=0)]$. However, if $L_{\mathrm{in}}>L_T$ (which is usually the case in metals), then one has to include the effects of energy averaging within a region of size L_{in}, which reduces the $\mathrm{Var}[g(L_{\mathrm{in}},T)]$ below it to a $T=0$ value. In addition, there is usually an intermediate temperature regime in metals when $L_{\mathrm{in}}>L>L_T$ where the T dependence of the sample variance only comes from energy averaging, but this effect is also found to have a nontrivial dependence on dimensionality. At a sufficiently low temperature, determined by the temperature at which both T-dependent lengths become longer than all sample dimensions, the behavior crosses over to the zero-temperature behavior described above and in Refs. 12 and 13.

It is convenient to calculate the temperature-dependent behavior from the $T=0$ behavior using the relation

$$g(T)=-\int dE\, f'(E,\mu)g(E)\ , \tag{3.2}$$

where

$$f'=\frac{df}{dE}=\frac{\beta e^{\beta(E-\mu)}}{(e^{\beta(E-\mu)}+1)^2}\ ,$$

f is the Fermi distribution function, $\beta=1/kT$, $g(E)=\mathrm{Tr}[t^{\dagger}(E)t(E)]$, and t is the transmission matrix defined above. Then

$$\begin{aligned}\bar{F}(\Delta\mu,\Delta B,T)&=\int dE_1\int dE_2\, f'(E_1,\mu)f'(E_2,\mu+\Delta\mu)\\&\quad\times\langle\delta g(E_1,B)\delta g(E_2,B+\Delta B)\rangle\\&=\int d\Delta E\, K(\Delta E,\Delta\mu)F(|\Delta E|,\Delta B)\ ,\end{aligned} \tag{3.3}$$

where $\delta g=g-\langle g\rangle$, and $K(\Delta E,\Delta\mu)$ is the convolution integral

$$K(\Delta E,\Delta\mu)=\int dE_1\, f'(E_1,\mu)f'(E_1-\Delta E,\mu+\Delta\mu)\ . \tag{3.4}$$

Note that in this approach the finite-T behavior is determined completely by the above integral over the zero T correlation function which we have calculated above, and requires no further diagrammatic analysis. Another approach, which is in principle more general, is to use the finite-temperature Green-function technique to reanalyze the diagrams as we do in Appendix B, where it is shown that both approaches give the same results. Here we adopt the simpler method of Eq. (3.3).

We begin by considering the case $\Delta\mu=0$. Then $\bar{F}(T)=\bar{F}(0,0,T)$ gives the mean-squared amplitude of the conductance fluctuations at a given temperature, $\mathrm{Var}[g(T)]$, and $\bar{F}(T,\Delta B)$ represents the magnetic field correlation function appropriate for comparison with experiment at that temperature. We also begin by assuming that $L_T<L_{\mathrm{in}}$, which is the typical situation in a metal at low T (in some systems, particularly MOSFET's, this inequality may be reversed, we will consider that case later). Since $f'(E,\mu)$ is large only for E within kT of μ, the function $K(\Delta E)$ appearing in (3.3) decays exponentially for $\Delta E>kT$. This function multiplies the $T=0$ energy correlation function $F(\Delta E)$ in the integrand of (3.3), which has a power-law asymptotic decay of the form $F(\Delta E)\sim(E_c/\Delta E)^{(4-d)/2}$, where $E_c=(\pi/2)hD/L^2$. If $kT<E_c$, then $K(\Delta E)$ has the narrower width in ΔE and may be further approximated by a δ function, giving $\bar{F}(T)\simeq F(\Delta E=0)$, the $T=0$ result whose values for $d=1,2,3$ were given above. We are now interested in the higher T regime where $kT>E_c$ (which is equivalent to the condition $L_T<L$). In this case, the function $K(\Delta E)$ in Eq. (3.3) only provides a sharp cutoff at kT to the integration over ΔE.

The perturbative expression for the function $F(\Delta E,L_{\mathrm{in}},\Delta B)$ is given by the sums in Eqs. (2.8) and (2.9). These are rather difficult to evaluate in closed form, and the results, which may be expressed in terms of derivatives of special functions, are not very useful. Therefore the simplest way of quantitatively comparing theory and experiment with no free parameters is to numerically evaluate the sums for $F(\Delta E,L_{\mathrm{in}},\Delta B)$ and then numerically perform the integrals in Eq. (3.3) for a given value of T. In what follows we will only evaluate the asymptotic dependences of $\bar{F}$ on the parameters $T,\Delta B,\Delta\mu$ in various regimes, and not numerical prefactors of order unity. Moreover, rarely in an experimental context will the corrections to the asymptotic dependences we calculate be negligible. We stress, therefore, that detailed quantitative agreement between theory and experiment should only be obtained by fitting to Eq. (3.3) evaluated numerically; although reasonable order-of-magnitude estimates can be obtained from the results to be given below. Some other important issues relevant to making detailed comparisons between theory and experiment will be discussed in Sec. III E below.

If we only wish to obtain the asymptotic behavior of $\bar{F}$ we can immediately simplify Eq. (3.3) by approximating

$$K(\Delta E)\simeq(1/kT)\theta(kT-\Delta E)\ .$$

We also replace $F(\Delta E, L_{\rm in}, \Delta B)$ by $F_1(\Delta E, L_{\rm in}, \Delta B)$ where F_1 is the contribution of the first diagram in Fig. 5 to F. It is easy to check that all the diagrams give the same asymptotic dependences, as one expects they should, since all diagrams diverge as the same power of the system size, and finite temperature simply introduces some shorter cutoff scale for these divergences. Finally, we express the integral in (3.3) in terms of dimensionless variables: $\eta = \Delta E / E_c$, $t = kT/E_c$, $\gamma = (L/\pi L_{\rm in})^2$, and begin by assuming $\Delta B = 0$.

B. Variance of $g(T)$

We first evaluate the typical size of the fluctuations expected at a given temperature in one, two, and three dimensions. We assume a cubic sample in each dimension, and postpone questions of dimensional crossover until later. Thus,

$$\bar{F}(T) \simeq \frac{1}{t} \int_0^t d\eta \, F_1(\eta, \gamma) \ . \tag{3.5}$$

As noted above, $F_1(\eta,\gamma)$ is a function which decays asymptotically as $\eta^{(d-4)/2}, \eta \gg \gamma$ and $\gamma^{(d-4)/2}, \gamma \gg \eta$. We are presently assuming $L_T < L_{\rm in} (\gamma < t)$, thus if F_1 decays slowly enough with η that the integral is dominated by the tail (values of order t), then one simply gets $\bar{F}(T) \sim t^{(d-4)/2} \sim (L_T/L)^{4-d}$ by power counting. On the other hand, in one dimension F_1 decays rapidly enough that the integral is dominated by values of η of order γ (or order unity if $\gamma < 1$) and this makes the one-dimensional results consistently different from those in two and three dimensions. In higher dimension $L_{\rm in}$ drops out of the problem entirely when $L_T < L_{\rm in}$, but not in one dimension. We will now demonstrate this behavior explicitly.

In one dimension the sums over m_x, m_y are omitted, and we can write

$$\bar{F}_{\rm 1D}(T) \sim \frac{1}{t} \sum_{m=1}^{\infty} \frac{1}{(m^2+\gamma)^2} \int_0^t d\eta \left[1 + \frac{\eta^2}{(m^2+\gamma)^2} \right]^{-2} . \tag{3.6}$$

Now we note that the integral over η is sharply cut off by the integrand when $\eta > (m^2+\gamma)$, hence the asymptotic behavior can be obtained by approximating the integrand by $\theta(1-x)$, where $x = \eta/(m^2+\gamma)$. This then yields two terms from the η integration:

$$\begin{aligned} \bar{F}_{\rm 1D}(T) &\sim \frac{1}{t} \sum_{m=1}^{\infty} \frac{1}{(m^2+\gamma)^2} [(m^2+\gamma)\theta(t-m^2-\gamma) \\ &\quad + t\theta(m^2+\gamma-t)] \\ &\sim \frac{1}{t} \left[\sum_{m=1}^{m_c} \frac{1}{(m^2+\gamma)} + t \sum_{m=m_c}^{\infty} \frac{1}{(m^2+\gamma)^2} \right] , \end{aligned} \tag{3.7}$$

where m_c is the largest integer less than $\sqrt{t-\gamma} \simeq \sqrt{t}$. For $\sqrt{t} \gg \sqrt{\gamma} \gg 1$ the first summation is $\sim \gamma^{-1/2}$, whereas the second is $\sim t^{-1/2}$, so we find

$$\bar{F}_{\rm 1D}(T) \sim \frac{1}{t\sqrt{\gamma}} + O(t^{-3/2}) \ .$$

The fact that the first correction to the leading asymptotic dependence is of order $\sqrt{\gamma/t} = L_T/L_{\rm in}$ illustrates that one is unlikely to achieve purely asymptotic behavior in an experimental context, because rarely is $L_{\rm in}$ more than an order of magnitude larger than L_T. Note also that the *next* order behavior corresponds to the result $\bar{F}_{\rm 1D}(T) \sim (L_T/L)^{(4-d)}$, the behavior expected from the above power-counting argument, which only fails in one dimension.

In two and three dimensions we can follow the same line of reasoning as above, using the θ-function approximation for the η integration, and simply replacing m^2 by $m_z^2 + m_x^2$ or by $m_z^2 + m_x^2 + m_y^2$, and the single summation over m in the two terms in Eq. (3.7) by a double (or triple) summation from $m_z = 1$, $m_x = 0 (m_y = 0)$. For $\gamma \gg 1$ we can change these multiple sums to spherically symmetric two- and three-dimensional integrals, giving

$$\bar{F}_d(T) \sim \frac{1}{t} \left[\int_1^{\sqrt{t-\gamma}} \frac{m^{d-1}}{(m^2+\gamma)} dm + \int_{\sqrt{t-\gamma}}^{\infty} \frac{m^{d-1}}{(m^2+\gamma)^2} dm \right] ,$$

thus

$$\bar{F}_{\rm 2D}(T) \sim \frac{1}{t} [\ln(t/\gamma) + 1]$$

and

$$\bar{F}_{\rm 3D}(T) \sim \frac{1}{t}\sqrt{t} \sim \frac{1}{\sqrt{t}} \ .$$

We see that up to a logarithmic correction in two dimensions, the inelastic length has dropped out of the temperature dependence as long as $L_{\rm in} > L_T$, and the asymptotic dependences on L_T are just those predicted by power counting.

Now, still considering the high-temperature regime, where both $L_T, L_{\rm in} \ll L$, suppose we have $L_{\rm in} < L_T$ (which is equivalent to $\gamma > t$). This situation is unusual in metals, but common in MOSFET's. In this case $F_1(\eta,\gamma) \sim \gamma^{(d-4)/2}$, independent of η in the integration range of Eq. (3.5), hence power counting works in all dimensions, and yields

$$\bar{F}_d(T) \sim \gamma^{(d-4)/2} \quad \text{for } \gamma \gg t \text{ and } d = 1,2,3 \ .$$

Remembering that the root-mean-squared fluctuation amplitude $\text{rms}[g(T)] = [\bar{F}(T)]^{1/2}$ and writing our results in terms of the T-dependent lengths, we can summarize the high-T behavior (where both L_T and $L_{\rm in}$ are shorter than the sample length) as follows:

$$\text{rms}[g(T)] \sim \frac{L_T}{L} \left[\frac{L_{\rm in}}{L} \right]^{1/2} \sim T^{(-1/2-p/4)} \quad \text{for } d = 1 \text{ and } L_T \ll L_{\rm in} < L_z \ , \tag{3.8a}$$

where $\tau_{\rm in}\sim T^{-p}$,

$$\mathrm{rms}[g(T)]\sim\left[\frac{L_T}{L}\right]^{(4-d)/2}\sim T^{(d-4)/4}\ \text{for } d=2,3 \text{ and } L_T\ll L_{\rm in}<L_z\ , \tag{3.8b}$$

$$\mathrm{rms}[g(T)]\sim\left[\frac{L_{\rm in}}{L}\right]^{(4-d)/2}\sim T^{p(d-4)/4}\ \text{for } d=1,2,3 \text{ and } L_{\rm in}\ll L_T<L_z\ . \tag{3.8c}$$

The results of Eqs. (3.8a) and (3.8b) have also been obtained by Al'tshuler and Khmel'nitskii in Ref. 14.

As we noted at the beginning, all these results are consistent with the picture that the system goes over to classical self-averaging on length scales longer than $L_{\rm in}$, hence we always find

$$\mathrm{rms}[g(L,T)]\simeq\mathrm{rms}[g(L_{\rm in})](L_{\rm in}/L)]^{(4-d)/2}$$

as long as $L_T,L_{\rm in}<L$. However, the temperature dependence of rms$[g(L_{\rm in})]$ is not necessarily equivalent to having coherent subregions on the scale L_T, i.e., it is *not* always true that when $L_T<L_{\rm in}$ we have rms$[g(L_{\rm in})]\sim(L_T/L_{\rm in})^{(4-d)/2}$ (which would make $L_{\rm in}$ cancel out of the result for rms$[g(T)]$). Equation (3.8a) shows that in one dimension rms$[g(L_{\rm in},T)]$ is not proportional to $(L_T/L_{\rm in})^{3/2}$, as expected by classical addition of resistors in series, but instead

$$\mathrm{rms}[g(L_{\rm in})]\sim L_T/L_{\rm in}=(E_c'/kT)^{1/2}\ ,$$

where $E_c'=hD/(L_{\rm in})^2$. Moreover, in the intermediate-temperature regime where $L_T<L<L_{\rm in}$ the above analysis leads to the replacement of $L_{\rm in}/L$ in Eq. (3.8a) by unity (*not* by L_T/L). So we find

$$\mathrm{rms}[g(T)]\sim\frac{L_T}{L}\sim(E_c/kT)^{1/2}\ \text{for } d=1 \text{ and } L_T\ll L\ll L_{\rm in}\ . \tag{3.9}$$

Although the self-averaging behavior introduced by thermal effects on the scale L_T are not equivalent to those caused by the classical self-averaging of resistor networks discussed above, they can be derived from a simple energy-averaging argument.[11,47,55] We will discuss the physical significance of these two different points of view below.

C. Dimensional crossover

Having determined the behavior of rms$[g(T)]$ in $d=1,2,3$, we next examine the conditions for dimensional crossover at finite temperature. We should note that since we are always considering finite-size conductors, the effective dimensionality at zero temperature is actually determined by the shape. If the sample length in the current direction, L_z, is much larger than in the transverse directions then the momentum sums in Eq. (2.9) are dominated by q_z (at the lower cutoff), and the important part of the sums correspond to the 1D eigenvalue problem. As soon as a transverse sample dimension becomes as large as L_z the important eigenvalues correspond to the 2D problem, and similarly for the 3D problem. Until now, in this section we have assumed that the samples were cubic in $d=2,3$ and ignored their width in the momentum sums in $d=1$. The correct general form of Eq. (3.6), for arbitrary shape (as discussed in Appendix A) replaces m_x^2 by $(L_z/L_x)^2m_x^2=s_xm_x^2$, and m_y^2 by $(L_z/L_y)^2m_y^2=s_ym_y^2$. To discuss the 1D to 2D crossover it is then convenient to separate out the terms with $m_x=m_y=0$ in Eq. (3.6), which give identically the 1D result, and write

$$\bar F(T)=\bar F_{\rm 1D}+\bar F_c(T)\ , \tag{3.10}$$

where

$$\bar F_c\sim\frac{1}{t}\int_0^t d\eta\sum_{m_x,m_y,m_z=1}^{\infty}\frac{(m_z^2+s_xm_x^2+s_ym_y^2+\gamma)^2}{[(m_z^2+s_xm_x^2+s_ym_y^2+\gamma)^2+\eta^2]^2}\ . \tag{3.11}$$

To consider 2D to 3D crossover one makes a similar separation of the terms with $m_y=0$ which gives exactly the 2D result, and the remaining terms which define the 2D to 3D crossover function. First, we consider the 1D to 2D crossover, so we omit the sum over m_y, and consider the case where $(s_x)^{1/2}\gg1$. To get the asymptotic behavior for $\gamma>1$ we can change the sums to integrals over continuous variables q_x,q_z with lower limit unity, and then rescale the variables to $\bar q_x=(s_x)^{1/2}q_x$, so the lower limit of the $\bar q_x$ integration is now $(s_x)^{1/2}$. The integrand is now spherically symmetric, and although the region of integration is not, we can ignore the small contribution from $1<q_z<(s_x)^{1/2}$. Defining $q^2=q_z^2+q_x^2$, we have

$$\bar F_c(T)=\frac{1}{t(s_x)^{1/2}}\int_0^t d\eta\int_{(s_x)^{1/2}}^{\infty}dq\,q\frac{(q^2+\gamma)}{[(q^2+\gamma)^2+\eta^2]^2}\ . \tag{3.12}$$

An exactly analogous derivation for the 2D to 3D crossover, assuming $s_x=1$, $(s_y)^{1/2}\gg1$ (a square film with a finite thickness), simply changes (3.12) to a 3D integral over q. Now using the θ-function approximation of (3.7) gives, for $d=2,3$,

$$\bar F_c(T)\sim\frac{1}{t}\left[\int_{\sqrt{s}}^{\sqrt{t-\gamma}}\frac{m^{d-1}}{(m^2+\gamma)}dm+\int_{\sqrt{t-\gamma}}^{\infty}\frac{m^{d-1}}{(m^2+\gamma)^2}dm\right], \tag{3.13}$$

assuming $t>\gamma,s$ (which is the nontrivial case). In two dimensions this gives $\bar F_c(T)\sim1/t\sqrt{s}$ which implies that for a rectanguar 2D sample

$$\begin{aligned}&\mathrm{Var}[g(T)]\sim\bar F_{\rm 1D}(T)+\bar F_c(T)\ ,\\ &\mathrm{Var}[g(T)]\sim(L_T/L_z)^2(L_{\rm in}/L_z+L_x/L_z)\ .\end{aligned} \tag{3.14}$$

Hence it follows that the 1D to 2D crossover occurs when the sample width L_x becomes shorter than $L_{\rm in}$. This is consistent with our findings above, that $L_{\rm in}$ is the relevant length in one dimension even if $L_T < L_{\rm in}$. For the 2D to 3D crossover again the situation is different, from (3.11) one finds

$$\mathrm{Var}[g(T)] \sim \frac{L_T}{L_z}(L_T/L_z + L_y/L_z) , \tag{3.15}$$

implying that the 2D to 3D crossover occurs when L_T becomes less than the thickness L_y. All this holds for $L_T < L_{\rm in}$; when $L_{\rm in} < L_T$ the dimensional crossover always occurs when $L_{\rm in}$ becomes shorter than the relevant transverse dimension. It should also be noted that the preceding analysis is still valid when a transverse dimension is longer than sample length in the current direction. Thus we see from Eqs. (3.14) and (3.15) that for such a sample the rms conductance fluctuations can be enhanced above their value for a cubic sample by a factor $(L_x L_y/L_z^2)^{1/2}$. For example, in the simple 2D case appropriate for MOSFET's, with $L_{\rm in} < L_T < L_z < L_x$, we have

$$\mathrm{rms}[g(T)] \sim \left[\frac{L_x}{L_z}\right]^{1/2} \frac{L_{\rm in}}{L_z} = \left[\frac{L_x}{L_{\rm in}}\right]^{1/2} \left[\frac{L_{\rm in}}{L_z}\right]^{3/2} .$$

This generalizes the result found at zero temperature, that for a sample which is much wider than it is long, the absolute magnitude of the conductance fluctuations can be much larger than e^2/h, and this effect has been seen experimentally recently, in good agreement with the above shape dependence.[9] It has been pointed out[41,9] that this behavior is just what one gets from treating the system as $L_x/L_{\rm in}$ parallel and $L_z/L_{\rm in}$ series classical resistors with fluctuations of order e^2/h occurring in each one.

D. Correlation ranges at finite temperature

Having discussed the amplitude of the fluctuations as a function of temperature in $d=1,2,3$ and the conditions for dimensional crossover, we are now in a position to discuss the scale of the fluctuations, i.e., the range of the correlation functions at finite T (at $T=0$ these were just B_c and E_c). The magnetic field correlation length $B_c(T)$ may be obtained with some modifications of the above analysis. Recall from the discussion in Sec. II that as long as the field difference ΔB in Eq. (2.13) could be treated as giving a perturbative correction to the eigenvalues of the diffusion equation, then the dimensionless field difference $b = \Delta B/B_c(0)$ gives an additive correction to the eigenvalues $\tilde{\lambda}$ in exactly the same way as does the dimensionless inelastic length γ [$B_c(0) \simeq \sqrt{3}\Phi_0/L_z L_y$]. Hence we have simply to replace γ by $\gamma + b$ in Eq. (3.5) and calculating in the same way as before, ask at what value of b is $\bar{F}(T,b) \simeq \frac{1}{2}\bar{F}(T,0)$. One sees immediately by replacing γ by $\gamma + b$ in Eqs. (3.8a)—(3.8c) that the crossover occurs at $b \sim \gamma$ in one dimension, when $L_T < L_{\rm in}$, and in all dimensions, when $L_{\rm in} < L_T$. Thus in one dimension the T dependence of the magnetic correlation length is always determined by the inelastic length, and until $L_{\rm in} < L_z$, the $T=0$ result for B_c holds. We saw above that the sample remains effectively 1D when $L_y, L_x < L_{\rm in} < L_z$, and we obtain from the condition $b \sim \gamma$,

$$B_c(T) \sim \frac{\phi_0}{L_{\rm in} L_x} \quad \text{for } d=1 \text{ and } L_y, L_x < L_{\rm in} < L_z , \tag{3.16}$$

where $\phi_0 = h/e$ and L_x is the sample dimension normal to both the field and the direction of current flow. This result holds independent of the relative size of L_T and $L_{\rm in}$. If $L_z, L_x > L_{\rm in} > L_y$, as may be the case when studying the longitudinal magnetoresistance of a thin metal film, then the sample is effectively 2D but the perturbative expression for the field-dependent eigenvalue $\tilde{\lambda}(\Delta B)$ still holds, since the eigenstates in the direction parallel to the field are independent of the field. So we can still use the approach of replacing γ by $\gamma + b$ to obtain $B_c(T)$. We find for the longitudinal magnetoconductance,

$$B_c(T) \sim \frac{\phi_0}{L_{\rm min} L_x} \quad \text{for } L_x < L_{\rm in} < L_y, L_z , \tag{3.17}$$

where $L_{\rm min} = \min(L_{\rm in}, L_T)$. This completely describes the behavior when the sample area normal to the field is effectively one dimensional because the width is less than the inelastic length.

Now we turn to the case where the inelastic length becomes shorter than the sample width, so that the sample is effectively two dimensional in the plane normal to the field. Now the eigenvalues and eigenvectors of (2.13) may no longer be obtained perturbatively from the solutions with $\Delta B = 0$, but instead they are approximately Landau levels with the effective cyclotron frequencies $\lambda_n = (n + \frac{1}{2})(D\Delta B/\phi_0)$.[60] This means that the eigenvalues appearing in (2.9) [and hence in (3.6)] have the form $\tilde{\lambda} = n\bar{b} + s_x m_x^2 + \gamma - i\eta$, where $\bar{b} = (\Delta B L_z^2)/\phi_0$, and these eigenvalues have degeneracy, $\delta = (\Delta B L_z L_x)/\phi_0$. If this replacement is made in Eq. (2.9), it is found that the $T=0$ correlation function does not decay rapidly enough in either the 2D or 3D case for the inelastic cutoff γ to enter $\bar{F}(T,\bar{b})$ when $L_T < L_{\rm in}$, and the field scale at which $\bar{F}$ begins to decay is $\bar{b} \sim t$, independent of L_y. On the other hand, when the inelastic length is the shortest length it always determines the crossover scale, so we find

$$B_c(T) \sim \frac{\phi_0}{L_{\rm min}^2} \quad \text{for } d=2,3 . \tag{3.18}$$

Thus once the sample cross section normal to the field is 2D, B_c is simply determined by the condition that the field difference correspond to a change in flux of order ϕ_0 through the area defined by the shorter of the two temperature-dependent lengths. It may appear that this result implies some inconsistency with the 1D to 2D dimensional crossover criterion, because Eqs. (3.16) and (3.18) suggest that once $L_{\rm in} < L_x$, B_c will change discontinuously to the potentially much larger field scale implied by Eq. (3.18). However, as our discussion of dimensional crossover made clear, at the crossover $\bar{F}(T)$ is the sum of two terms of approximately equal size corresponding to the 1D and 2D results. The 1D term will have the short scale and the 2D term the long one; right at the

crossover their amplitudes are comparable and the correlation function should reflect both scales. Only far from the dimensional crossover will one or the other term be negligible, so the correlation functions will not change scale discontinuously.

Now we consider the correlation length in chemical potential at finite T. At finite T it is important to distinguish between chemical potential and electronic energy. What we have called the energy correlation function at $T=0$ is really the correlation of conductances at two different chemical potentials. To calculate the finite-T generalization we must start over from Eq. (3.3), setting $\Delta B=0$. We are looking for the decay length of $\bar{F}$ with $\Delta\mu$ which we denote by μ_c. If $\Delta\mu<kT$ then we can still make the approximation that $K(\Delta E,\Delta\mu)\simeq\theta(kT-\Delta E)$, and proceed with the line of analysis used above. However, when $\Delta\mu$ becomes greater than kT, $K(\Delta E,\Delta\mu)$ already decays exponentially with $\Delta\mu/kT$ for all values of ΔE. Hence μ_c can never be much larger than kT, no matter what the relationship of L_T to $L_{\rm in}$ (kT to $h/\tau_{\rm in}$). This means we do not have to consider the case $L_{\rm in}<L_T(\gamma>t)$ in the subsequent analysis. With this in mind, we retrace the analysis which led to (3.5) and find that the only modification that occurs when $\Delta\mu$ is nonzero is in the limits of the integration:

$$\bar{F}(T,\tilde{\mu})\sim\frac{1}{t}\int_{\tilde{\mu}}^{t+\tilde{\mu}}d\eta\,F_1(\eta,\gamma)\,, \tag{3.19}$$

where $\tilde{\mu}=\Delta\mu/E_c$. Using again the approximation of the integrand employed in (3.7) we can evaluate $\bar{F}$ asymptotically, and find its crossover behavior with $\tilde{\mu}$. Not surprisingly, this is the same as the crossover behavior of $B_c(T)$ when $L_T<L_{\rm in}$. Thus in one dimension the crossover occurs when $\tilde{\mu}\sim\gamma$, whereas in $d=2,3$ it occurs when $\tilde{\mu}\sim t$. Therefore

$$\mu_c(T)\sim h/\tau_{\rm in}\ \text{ for } d=1 \text{ and } L_T<L_{\rm in}<L_z\,, \tag{3.20a}$$

$$\mu_c(T)\sim kT\ \text{ for } d=1 \text{ and } L_{\rm in}<L_T<L_z\,, \tag{3.20b}$$

$$\mu_c(T)\sim kT \text{ for } d=2,3 \text{ and } L_T,L_{\rm in}<L_z\,. \tag{3.20c}$$

In quasi-1D MOSFET's, the system where it is easiest to study fluctuations of the conductance with chemical potential, typically $h/\tau_{\rm in}\simeq kT$, so one always expects the typical fluctuation scale to be order kT.

E. Experimental observability of the fluctuations

At this point it is worth examining in detail what these results imply about the experimental observability of these effects at higher temperatures, and in larger systems than the ultrasmall conductors where the effects have been clearly seen at temperatures of a few degrees kelvin and below. We note that according to Eq. (3.8) the total fluctuation amplitude, rms$[g(T)]$, decreases with increasing temperature as a very slow power law, typically in the range of $T^{-1/2}$ to $T^{-1/4}$. This suggests that the conductance fluctuations should be observable at substantially higher temperatures. On the other hand, the experimentally observed conductance fluctuations as a function of magnetic field, or chemical potential, appear to wash out with temperature very rapidly, so that in many experiments the effect is apparently unobservable above a few degrees kelvin. In particular, Licini *et al.*[7] followed the temperature dependence of a particular feature in the magnetoconductance, and observed a much more rapid decrease with temperature than is consistent with the weak power laws derived above. The resolution of this inconsistency lies in the observation that as the temperature rises the correlation field $B_c(T)$, given by Eqs. (3.17) and (3.18) increases. Suppose the experimentalist is observing two features separated by a distance in magnetic field ΔB. Then Eq. (3.8) for rms(g) will only give the typical difference in conductance between those two points if $\Delta B\gg B_c(T)$. As the temperature continues to rise eventually $B_c(T)$ exceeds ΔB, at which point the values of the magnetoconductance over the entire range ΔB are correlated and will have much smaller fluctuations in amplitude. To make this argument a little more quantitative, we introduce the quantity

$$\delta\tilde{g}(\Delta B)=\tfrac{1}{2}\langle[\delta g(B)-\delta g(B+\Delta B)]^2\rangle^{1/2}\,, \tag{3.21}$$

where $\delta g=g-\langle g\rangle$, as a measure of the amplitude of the fluctuations in $g(B)$ on fixed scale ΔB. For $\Delta B\gg B_c(T)$, $\delta\tilde{g}(\Delta B)\simeq$rms$[g(T)]$, because the cross terms in Eq. (3.21), which are simply proportional to $F(\Delta B)$, have decayed to zero. However, for $\Delta B\ll B_c$, F is not small and we may expand it approximately as

$$F(\Delta B)\simeq\mathrm{Var}(g)[1-\tfrac{1}{2}(\Delta B/B_c)^2]\,, \tag{3.22}$$

which should be approximately valid up to $\Delta B\simeq B_c$, where by definition F has decreased by a factor of 2. Combining Eqs. (3.21), and (3.22), we find

$$\delta\tilde{g}\simeq\tfrac{1}{2}\mathrm{rms}[g(T)][\Delta B/B_c(T)] \tag{3.23}$$

for $\Delta B<B_c(T)$. The factor $\Delta B/B_c(T)$ introduces a further temperature dependence which makes the difference in conductance of two field points separated by a distance ΔB decrease much more rapidly with increasing temperature, once ΔB becomes less than $B_c(T)$. It is precisely this sort of quantity, the difference of two nearby extrema in the conductance, which was measured in the experiment of Licini *et al.* For that experiment, which is in the 2D limit, Eq. (3.23) predicts a crossover from a $T^{-1/2}$ decrease, to a $T^{-3/2}$ decrease as B_c exceeds the spacing of the peak and valley at low temperature. In Fig. 12 we superimpose these temperature dependences on the data of Licini *et al.*, and find that the agreement is satisfactory. The order of magnitude of the cross-over field also is in agreement with the result expected for this system, $B_c(T)\sim\phi_0/L_{\rm in}^2$. Obviously similar ideas apply to the conductance fluctuations as a function of chemical potential at a fixed spacing $\Delta\mu$.

However, if one analyzes full magnetoconductance traces ("magnetofingerprints"), where the total field range is many times $B_c(T)$ at all temperatures, and calculates the rms fluctuations of $g(B)$ around the mean, *this* quantity should show the much weaker temperature dependence predicted by Eq. (3.8). Unfortunately, for an inelastic mean free path of 1000 Å, $B_c(T)$ becomes of order several tesla, so there will not be enough of a field range available to perform traces much longer than $B_c(T)$.

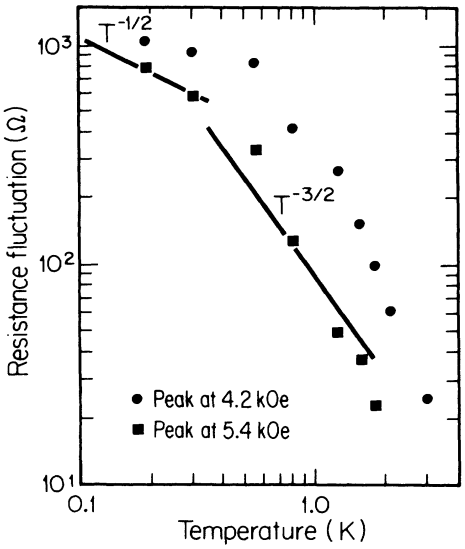

FIG. 12. Behavior of the peak-to-valley fluctuation amplitude of two structures at magnetic fields of 4.2 and 5.4 KOe versus temperature [data from Licini *et al.* (Ref. 7)]. The straight lines represent the theoretical prediction described in Sec. III F of a crossover from $T^{-1/2}$ at low temperature to $T^{-3/2}$ at higher temperature. The crossover occurs when $B_C(T)$ becomes comparable to the magnetic field difference.

Hence, as mentioned in the Introduction, it will be difficult to measure the conductance fluctuations by looking at room-temperature magnetoconductance, even though the rms value of the fluctuations should only decrease by 1 or 2 orders of magnitude from its low-temperature value. However, it should be possible to observe the fluctuations at room temperature if it is possible to vary some sample parameter other than the magnetic field enough to produce uncorrelated values of the conductance. The most attractive possibility would be to make controlled changes in the impurity configuration, and observe the induced fluctuations in g. Recent theoretical work has shown that for very dirty metals fluctuations as large as e^2/h can be induced by such small changes,[44,61] and these would have essentially the same weak temperature dependence as the fluctuations caused by going to an entirely different sample. Indeed, it has been suggested that the amplitude of room-temperature $1/f$ noise in dirty metals can be explained as arising from small intrinsic sample changes of this type.[44]. Furthermore, while the above discussion suggests that it will be difficult to observe magnetoconductance fluctuations in either small or large samples at high temperature, the same does *not* apply to large samples at low temperatures. At fixed temperature the field correlation length will remain constant and at low T will be much shorter than the available field range. Then increasing the size of the sample will only induce the slow classical self-averaging, with $\text{rms}(g)\sim(L_{\text{in}}/L)^{(4-d)/2}$. This suggests the magnetoconductance fluctuations will be observable, for example, in thin metal strips which can be hundreds of microns long.

A final complication in comparing theory and experiment quantitatively regards the difficulty in obtaining statistically meaningful values for the correlation functions. The correlation function must be calculated from a finite set of data points, where the number of uncorrelated values of $g(B),g(\mu)$ is roughly the total range of field or chemical potential in the data set divided by B_c or μ_c. Typically this number is about 10 to 50, which provides good enough statistics to expect to measure the amplitude of the correlation function with 10% to 50% accuracy, but not good enough to provide reliable statistics for the tail of the correlation function, which is thus liable to have meaningless oscillations. The best way to avoid this is probably to measure $g(B)$ at many uncorrelated values of the chemical potential as is possible in MOSFET's,[9] but in general it will take some care and effort to measure the long-range correlations in the tail predicted above, and even the value of $\text{rms}[g(T)]$ will not be easy to measure with high accuracy.

F. Physical interpretation of the temperature dependence

In conclusion, we make some comments about the interpretation of these results. Above we saw that when L_{in} was the shortest length scale, the T dependences of all our results were consistent with those expected by the hypothesis that the statistical behavior of the conductance becomes classical beyond that length scale. The same was not true of L_T, which was most clearly demonstrated by the result (3.9), which predicts $\text{rms}[g(T)]\sim T^{-1/2}$ in one dimension, and not the $T^{-3/4}$ expected by classical reasoning. The point raised here is that the two lengths L_T and L_{in} have very different physical significance. L_{in} represents inelastic processes which introduce a *dynamic* phase incoherence into the electronic motion, thus it defines a spatial region within which the electron is likely to propagate with a well-defined phase at a given energy. This sets the scale of the largest spatial region where electrons can interfere in a fixed, time-independent manner, whether the inteference is of the stochastic type represented by the fluctuations or the nonrandom type described by weak localization theory. L_T, on the other hand, represents a kind of *static* phase randomness in the electronic transport. If one thinks of the probability that an electron propagates diffusively between two points on opposite sides of the system as a sum of Feynman paths, then as discussed in the Introduction these amplitudes will have fixed but arbitrary phase for a given energy, but these relative phases will fluctuate in a deterministic way as the energy is changed. The energy scale for these fluctuations is hD/L^2, hence $L_T=(hD/kT)^{1/2}$ defines the largest system where thermal smearing of electronic energies over a range kT will not mix uncorrelated energies in the sum over paths. If the system is larger than L_T, even though there is no dynamic change in the phase of the electron as it traverses the system, there will still be $kT/E_c=(L/L_T)^2$ "independent" electronic energies participating in conduction, leading to a partial self-averaging of the $T=0$ fluctuations.[11,47,55] If two energies separated by more than E_c were truly statistically independent, then this energy-averaging argument would al-

ways correctly predict a $(E_c/kT)^{1/2}$ reduction of rms(g) when $L_T < L, L_{\rm in}$ [or a $(E_c'/kT)^{1/2}$ reduction when $L_{\rm in} < L$, where $E_c' = hD/L_{\rm in}^2$]. However, only in one dimension does the energy correlation function decay rapidly enough that two energies separated by more than E_c are really effectively independent (two dimensions is the marginal case), and so only in one dimension does the simple energy-averaging picture hold. On the other hand, since inelastic scattering does really introduce total spatial phase incoherence beyond a given length scale, we certainly expect that when $L_{\rm in}$ is the shortest length scale, we should get the classical result, which is indeed the result obtained in Eq. (3.8c). It is worth noting that in this context it is clear why the weak localization effects are not reduced by this energy averaging. It is now well understood that weak localization effects arise from constructive interference of a special subset of the Feynman paths contributing to backscattering, pairs of paths which go into one another upon time reversal. Such pairs have a fixed relative phase (zero at $B=0$), independent of energy, so averaging over many energies separated by more than E_c does not introduce any phase cancellation, and thus does not lead to self-averaging in the sum over paths.

Finally, we note that for the T dependence of the fluctuations, the physical difference between inelastic scattering and energy averaging only leads to a small change in the slow power-law decay of the fluctuations. However, for the h/e Aharonov-Bohm effect in metal rings, which is also a fluctuation effect of order e^2/h,[13,14,46,47] the difference is crucial, because this effect requires that some definite phase be preserved while an electron traverses the *entire* circumference of the ring. Hence the effect is destroyed exponentially by inelastic scattering, whereas it is only reduced as $(E_c/kT)^{1/2} \sim L_T/2\pi r$ by energy averaging. If the effect had decreased exponentially with L/L_T, it would have been much more difficult to detect experimentally. In fact the experiments find a weak temperature dependence in good agreement with the $T^{-1/2}$ behavior predicted by energy averaging.[3,4]

We summarize the results of this section as follows. First, the amplitude of the conductance fluctuations decreases with increasing temperature as a slow power law, rms$[g(T)] \sim T^{-\alpha}$, where typically $\frac{1}{4} \le \alpha \le \frac{3}{4}$. This decrease occurs when the relevant T-dependent length scales become shorter than the sample length. The detailed dependences in each dimension, as well as the conditions for dimensional crossover are determined by the interplay of the two length scales $L_T = (hD/kT)^{1/2}$ and $L{\rm in} = (D\tau_{\rm in})^{1/2}$. The typical scale of the fluctuations in magnetic field and chemical potential increases with increasing T, roughly consistent with the picture that the effective sample size is determined by the appropriate T-dependent length scale. Detailed results for all these quantities at finite temperature are summarized in Table I. In this table $L_{\rm min}$ is the shorter of $L_T, L_{\rm in}$, L_t is the relevant direction transverse to the current direction (L_z), and $\phi_0 = h/e$ is the quantum of flux. Also, all quantities have a numerical coefficient of order unity, and the behavior of rms$[g(T)]$ is given for a cubic sample of size L (shape dependence at finite temperature is discussed at the end of Sec. III C).

IV. CONCLUSIONS

The main results of this paper are that the conductance fluctuations, which have a universal amplitude at zero temperature, decrease slowly with increasing temperature for a sample of fixed size, or slowly with size for a sample at fixed, nonzero temperature. The results are roughly consistent with the picture that the sample behaves classically when observed on scales much longer than the inelastic length, and that the scale of the fluctuations is thus determined by the largest phase-coherent subregion of the sample. However, there are important corrections to this simple picture which arise from energy averaging and long-range correlations in energy, as discussed in the preceding section. Electron-electron interactions do not significantly alter our results at zero temperature, and at finite temperature only appear as a contribution to the inelastic scattering. The fluctuation effects have a different origin from weak localization effects, and at sufficiently low temperatures will mask those effects in small samples. The fluctuations also present an interesting analogy to the level fluctuations studied in nuclear physics, particularly the phenomenon of Ericson oscillations, but the two effects are not identical. However the universality of the fluctuation amplitude may still be related to the eigenvalue rigidity of random matrices, as discussed in Refs. 41 and 42.

Although the universal amplitude of the conductance fluctuations in metals is a surprisingly general result, it might have been anticipated in two cases, based on the ideas of the scaling theory of localization. In the 2D metallic regime the conductance itself is approximately scale independent (by Ohm's law), and since g is the only scaling variable, its fluctuations must also be scale independent.[72] Near the metal-insulator transition in three dimensions the conductance is also scale independent, so again its fluctuations should be independent of size.

Nonetheless, as we have emphasized above, the universal size-independent amplitude of the fluctuations in all dimensions is surprising, both on the basis of classical reasoning, and on the basis of the natural assumption that the probability of propagating across the sample to widely separated end points should be statistically independent. The universal conductance fluctuations thus imply some

TABLE I. Finite-temperature results.

Conditions	rms$[g(T)]$	B_c	μ_c	$d \to d+1$
$d \ge 2$, $d=1$, $L_{\rm in} < L_T, L_z$	$(L_{\rm min}/L)^{(4-d)/2}$	$\phi_0/L_{\rm min}^2$	kT	$L_t > L_{\rm min}$
$d=1$, $L_T < L_{\rm in} < L_z$	$(L_T/L)(L_{\rm in}/L)^{1/2}$	$\phi_0/L_t L_{\rm in}$	$h/\tau_{\rm in}$	$L_t > L_{\rm in}$
$d=1$, $L_T < L_z < L_{\rm in}$	L_T/L	$\phi_0/L_z L_t$	kT	$L_t > L_z$

subtle and potentially long-range spatial correlation in the transmission probabilities to different points across the sample which deserves further study. In this context, it is important to note that the universal transmission fluctuations are not a quantum-mechanical effect in any sense except for the importance of the phase coherence of the electrons. The same statistical behavior should be seen in any systems in which approximately monoenergetic waves are diffusing in a static, random potential; in particular, such behavior should be observable in classical wave systems, such as light scattering in a dense static random medium, or third sound in liquid helium. In these systems it should be possible to look not only at fluctuations in the integrated transmission $[\mathrm{Tr}(tt^{\dagger})]$, but at the spatial intensity distribution (speckle pattern), in order to observe directly the spatial correlations leading to the universal conductance fluctuations. It should be emphasized strongly that the simple observation of large relative fluctuations in spatial intensity, independent of size, is not sufficient to corroborate the main idea of the universal conductance fluctuations. As noted in the Introduction, such large relative fluctuations are always to be expected when the amplitude at a given point is the sum of many uncorrelated amplitudes. This sort of fluctuation phenomenon has been known in classical wave scattering at least since the time of Rayleigh.[73] The interesting new phenomenon which manifests itself in the universal conductance fluctuations is that there exists a long-range correlation in the speckle pattern which means that the intensity fluctuations in widely-separated regions in space are *not* statistically independent. Another way of saying this is that the common assumption in disordered systems, that an ensemble average is equivalent to a spatial average, fails badly in this case. The detailed behavior of this subtle long-range correlation in the speckle pattern is presently being studied, and these results will be presented elsewhere.[74]

It should also be pointed out that (for any fixed configuration of the scattering potential) the fluctuations in the speckle pattern may mask the weak localization effects which have been predicted to occur in classical systems also.[75] The recent experiments[76,77] which reported the observation of weak localization of light apparently avoided this problem by time averaging the signal from a suspension of mobile scatterers, a procedure which effectively ensemble averages the scattering behavior.

We have also emphasized that the universal amplitude of the fluctuations leads to a non-self-averaging behavior of the conductance in one and two dimensions in the sense that the fractional variance, $\mathrm{Var}(g)/\langle g\rangle^2$, does not go to zero as the system size goes to infinity. By our ergodic hypothesis this can lead to various types of reproducible sample-specific behavior of the conductance as a function of external parameters such as the "magnetofingerprints" discussed above. It is natural to ask how sensitive such sample-specific characteristics are to small intrinsic changes in the sample. This question has been answered recently;[44,62] it has been shown that the conductance is extraordinarily sensitive to small changes in the sample configuration. In fact, in two dimensions the rms change induced by moving just a single strong scatterer, $\delta G_1 \sim (k_F l)^{-1/2} e^2/h$, independent of system size (and the effect is even larger in one dimension).[78] Because of this one can regard the conductance, or the magnetofingerprint as a probe of the microscopic structure of samples which are macroscopically identical. Changes in the conductance will directly reflect microscopic changes in the impurity configuration, or sample characteristics. This may be very useful in obtaining information about such phenomena as tunneling in metallic glasses, slow dynamic phenomena in glassy systems, charge-density-wave distortion and depinning, and $1/f$ noise. Indeed, in Ref. 44 it was argued that this theory of the conductance fluctuations induced by small intrinsic changes in the sample provides a microscopic technique by which the amplitude of $1/f$ noise in dirty metals can be derived, when combined with the assumptions of the standard models. If this is correct, then these "quantum" fluctuation phenomena actually have important consequences for room-temperature conductance, as noted in our Introduction.

Finally, experimental attempts to measure these fluctuations are likely to again raise the fundamental issue of what exactly is measured in a resistance measurement. For example, the theory is done for a sample of well-defined size connected to perfectly conducting "leads;" experiments are almost always done at fixed current with voltage leads attached at various points along the sample. There is no reason that the voltage drop measured between two such points should be regarded as a local property of the region between the voltage probes.[79] In fact, our theory suggests that a variety of nonlocal effects should be present. For instance, if the inelastic length is much longer than the distance between the probes, the "sample area" relevant to the scale of the magnetic field fluctuations should also be much larger than the area between the probes. There are indications that this effect has already been seen.[9] Also, as noted in Sec. II, it has been shown[14] that there are fluctuations in g_{xy} of order unity, when a current is run in the x direction, even in the absence of a magnetic field. Thus two probes on opposite sides of a wire, with a current running perpendicular to the line joining them, will still develop a voltage drop. This is just one example of the violations of expected symmetry relations which can occur in systems which exhibit these fluctuation phenomena. It will be of great interest both experimentally and theoretically to develop a full understanding of these and other nonlocal and anisotropic effects which influence the results of transport measurements on small conductors.

ACKNOWLEDGMENTS

We gratefully acknowledge useful discussions with Y. Imry, M. Kastner, S. Kivelson, W. Skocpol, S. Washburn, and R. Webb. H. Fukuyama is grateful for the support of the Department of Physics, Massachusetts Institute of Technology and IBM Thomas J. Watson Research Center (Yorktown Heights, NY) for visits during which some of this work was done. P.A.L. acknowledges the support of the National Science Foundation under Grant No. DMR-82-17956. A.D.S. acknowledges financial support by IBM and thanks IBM for the use of their computational facilities.

APPENDIX A: EVALUATION OF THE ZERO-TEMPERATURE DIAGRAMS

In order to evaluate F quantitatively to obtain the absolute magnitude of the conductance fluctuations, we must evaluate Eq. (2.3) for a finite sample. Thus the diagrams must be formulated in real space. Let us first consider Fig. 5(a). There are, in fact, four possibilities for the arrangements of G^+ and G^- which are shown in Figs. 13(a)–13(d). Consider Fig. 13(a) first. We have

$$F_a=\left[\frac{1}{m^2L_z^2}\right]^2 N_a\int d\vec{r}_3\int d\vec{r}_4\int d\vec{r}_5\int d\vec{r}_6(c_iu^2)^2P(\vec{r}_6,\vec{r}_5)P(\vec{r}_4,\vec{r}_3)j(\vec{r}_3,\vec{r}_6)j(\vec{r}_4,\vec{r}_5)\ , \tag{A1}$$

where N_a is a counting factor to be determined later, and P is the diffusion propagator which will also be discussed later. The factor c_iu^2 ensures that the impurity ladder contains at least one impurity line. The factor j represents the part of Fig. 13(a) isolated in Fig. 14(a). It is an integral over $\vec{r}_1$ and $\vec{r}_2$ of a product of four G's with the appropriate spatial derivatives associated with the current vertex that are shown in Eq. (2.5). To evaluate j we note that $\langle G(\vec{r}_1,\vec{r}_2)\rangle$ decays exponentially on a distance scale of the mean free path, which is the shortest distance scale in the problem. This means that $\vec{r}_3$ and $\vec{r}_6$ must also be within l of each other for j to be appreciable. To the accuracy that we need, we may write

$$j=j_0\delta(\vec{r}_3-\vec{r}_4) \tag{A2}$$

and evaluate $j_0=V^{-1}\int d\vec{r}_3d\vec{r}_6j(\vec{r}_3,\vec{r}_6)$ where V is the volume. At this point j_0 can be evaluated in momentum space because $\langle G(\vec{r}_1\vec{r}_2)\rangle$ and therefore $j(\vec{r}_3,\vec{r}_6)$ are approximately translationally invariant as long as $L_z\gg l$. The result is

$$j_0=\int\frac{d\vec{p}}{(2\pi)^d}p_z^2G_+^2(p)G_-^2(p)$$
$$=\frac{k_F^2}{d}N_0 4\pi\tau^3\ . \tag{A3}$$

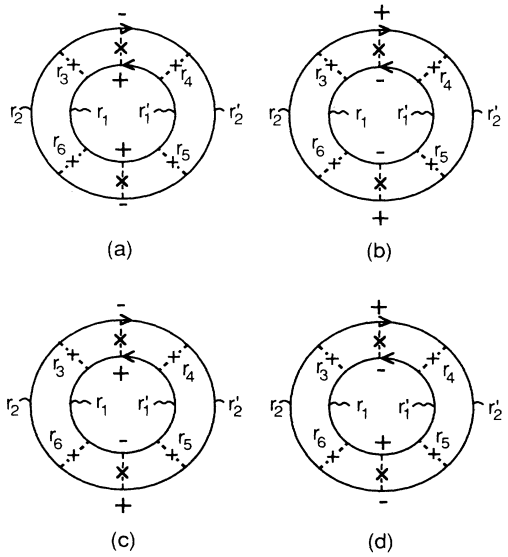

FIG. 13. More detailed representation of Fig. 5(a) showing the different arrangement of the advanced and retarded Green's functions (indicated by plus and minus signs).

Note that Eq. (A3) is simply what one would have gotten if one evaluated Fig. 14(a) in momentum space and associate a factor p_z with each current vertex. The short-range nature of j corresponds to neglecting the momentum q associated with the particle-hole line compared with k_F in the evaluation of Fig. 14(a). We prefer the present formulation, because in order to take into account finite-size effects quantitatively it is necessary to work in real space, and also because of subtle complications we will soon encounter in the evaluation of Figs. 5(b) and 5(c).

Returning to Eq. (A1), the diffusion propagator $P(\vec{r}_4,\vec{r}_3)$ describes the propagation of density fluctuation from $\vec{r}_3$ to $\vec{r}_4$ and satisfies the following diffusion equation:

$$(-D\nabla^2-i\,\Delta E+\tau_{\rm in}^{-1})P(\vec{r},\vec{r}\,';\Delta E)=(1/\tau)\delta(\vec{r}-\vec{r}\,')\ . \tag{A4}$$

For an infinite sample, we have translational invariance and Eq. (A4) can be solved by Fourier transform to yield

$$P(q,\omega)=\frac{1}{\tau(Dq^2-i\omega+\tau_{\rm in}^{-1})}\ . \tag{A5}$$

For finite samples, however, Eq. (A4) must be solved subject to the following boundary conditions. When the sample is in contact with vacuum or an insulator, there is no current flow normal to the boundary and the boundary condition is

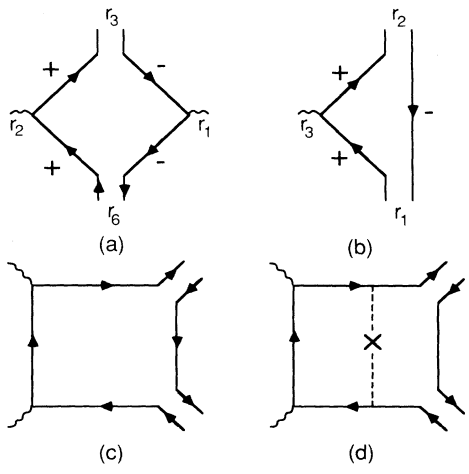

FIG. 14. (a) The vertex part of Figs. 5(a) and 13. (b) The vertex part of Fig. 5(b). (c) and (d) The vertex part of Figs. 5(d) and 5(e).

$$\frac{\partial}{\partial r_\perp} P(\vec{r},\vec{r}\,')=0 . \tag{A6a}$$

On the other hand, when the sample is connected to a good metallic contact with infinite conductivity, the boundary condition on the boundary $\vec{r}_B$ is

$$P(\vec{r}=\vec{r}_B,\vec{r}\,')=0 . \tag{A6b}$$

Equation (A4) is solved by writing

$$P(\vec{r},\vec{r}\,';\Delta E)=\sum_m \frac{Q_m^*(\vec{r})Q_m(\vec{r}\,')}{\lambda_m} , \tag{A7}$$

where Q_m and λ_m are the normalized eigensolution of

$$\tau(-P\nabla^2 - i\,\Delta E + i\tau_{\rm in}^{-1})Q_m=\lambda_m Q_m \tag{A8}$$

subject to the boundary condition $\partial Q_m/\partial \vec{r}_\perp=0$ or $Q_m(\vec{r}=\vec{r}_B)=0$ as discussed above. Let us consider a block $L_x\times L_y\times L_z$ with ideal leads in the z direction, then clearly $m=\{m_x,m_y,m_z\}$, where $m_x,m_y=0,1,2,\ldots,\infty$ and $m_z=1,2,\ldots,\infty$ and

$$Q_m=\left[\frac{L_x}{2}\frac{L_y}{2}\frac{L_z}{2}\right]^{-1/2}\sin(m_z\pi z/L_z)$$

$$\times\cos(m_x\pi x/L_x)\cos(m_y\pi y/L_y) . \tag{A9}$$

The eigenvalue is

$$\lambda_m=\tau D\left[\frac{\pi}{L_z}\right]^2\left[m_z^2+m_x^2\frac{L_z^2}{L_x^2}+m_y^2\frac{L_z^2}{L_y^2}\right]-i\tau\,\Delta E+\tau\tau_{\rm in}^{-1} . \tag{A10}$$

Now we have everything we need to evaluate Fig. 13(a) apart from the counting factor N_a. We simply note that exchanging r_1 and r_1' in Fig. 13(a) should be considered distinct diagrams. Thus we have $N_a=2$. Setting Eqs. (A3) and (A7) into (A2) and using the orthogonalities of the Q_m's, we obtain for Fig. 13(a)

$$F_a=\frac{2}{L_z^4}\left[\frac{v_F^2}{d}N_0 4\pi\tau^3\right]^2 c_i^2 u^4\sum_m\frac{1}{\lambda_m^2} . \tag{A11}$$

The constants can be greatly simplified using the fact that $\tau^{-1}=2\pi c_i u^2 N_0$ and $D=v_F^2\tau/d$. It is useful to introduce the energy scale

$$E_c=D(\pi/L_z)^2 \tag{A12}$$

and define

$$\tilde{\lambda}_m=\lambda_m/(E_c\tau)$$
$$=m_z^2+m_x^2(L_z^2/L_x^2)+m_y^2(L_z^2/L_y^2)-i\eta+\gamma , \tag{A13}$$

where

$$\eta=\Delta E/E_c \tag{A14a}$$

and

$$\gamma=(\tau_{\rm in}E_c)^{-1} . \tag{A14b}$$

Then Eq. (A11) can be written as

$$F_a=\left[\frac{4}{\pi^2}\right]^2\sum_{m_x,m_y=0}^{\infty}\sum_{m_z=1}^{\infty}\tilde{\lambda}_m^{-2} . \tag{A15}$$

Evaluation of Figs. 13(b), 13(c), and 13(d) proceeds in the same way except that we must recognize that upon exchanging + and − in the diffusion propagation, we effectively change the sign of ΔE and $\tilde{\lambda}_m\to\tilde{\lambda}_m^*$. The sum of Figs. 5(a)–5(d) can be labeled as $F_{5(a)}^{(\rm ph)}$ where

$$F_{5(a)}^{(\rm ph)}=2\left[\frac{4}{\pi^2}\right]^2\sum_{m_x,m_y=0}^{\infty}\sum_{m_z=1}^{\infty}[{\rm Re}(\tilde{\lambda}_m^{-1})]^2 . \tag{A16}$$

We next turn our attention to Fig. 5(b). The new feature is the appearance of the current vertex which is isolated in Fig. 14(b). Denoting it by $j_1(r_1,r_2)$, we can again approximate it by a translational invariant quantity $j_1(r_1-r_2)$ as long as $l\ll L_z$. We denote its Fourier transform by $j_1(q)$ which can be evaluated using the standard rules in momentum space

$$\bar{j}_1(\vec{q})=\sum_p p_z G_+(p)G_+(p)G_-(\vec{p}+\vec{q}) , \tag{A17}$$

where we have associated the momentum p_z with the current vertex. Equation (A17) is evaluated by expanding $G_-(\vec{p}+\vec{q})$ to linear order in q, i.e.,

$$G_-(\vec{p}+\vec{q})=G_-(p)+(\vec{p}\cdot\vec{q}/m)G_-^2(p) .$$

We then obtain

$$\bar{j}_1(\vec{q})=-q_z C_1 , \tag{A18}$$

where $C_1=(k_F^2/dm)N_0 4\pi\tau^3$.

Returning to real space, we have

$$j_1(\vec{r}_1-\vec{r}_2)=\int\frac{d\vec{q}}{(2\pi)^d}e^{i\vec{q}\cdot(\vec{r}_1-\vec{r}_2)}q_z C_1$$
$$=\frac{1}{i}\frac{d}{dr_{1,z}}\int\frac{d\vec{q}}{(2\pi)^d}e^{i\vec{q}\cdot(\vec{r}_1-\vec{r}_2)}C_1$$
$$=(C_1/i)\frac{d}{dr_{1,z}}[\delta(\vec{r}_1-\vec{r}_2)] . \tag{A19}$$

The value of Fig. 5(b) is given as follows:

$$F_{5(b)}^{(\rm ph)}=N_b\left[\frac{1}{m^2L_z^2}\right]^2\int d\vec{r}_1\int\cdots\int d\vec{r}_6(c_i u^2)^3 P(\vec{r}_1,\vec{r}_2)j_1(\vec{r}_2,\vec{r}_3)P(\vec{r}_3,\vec{r}_4)j_1(\vec{r}_4,\vec{r}_5)P(\vec{r}_5,\vec{r}_6)j(\vec{r}_6,\vec{r}_1)+{\rm c.c} . \tag{A20}$$

The counting factor $N_b=8$ corresponding to different ways of arranging the current vertices with three diffusions. The Green's function on the inner and outer loops are advanced and retarded, or they can be retarded and advanced, account-

ing for the complex conjugate term in Eq. (A20). In the evaluation of Eq. (A20), we use Eq. (A19) for j_1 and perform an integration by parts to transfer the d/dr_z to the function P. Using the δ function, we end up with integrals of the type

$$\int d\vec{r}_1 \int d\vec{r}_2 \int d\vec{r}\, P(\vec{r},\vec{r}_1)\frac{\partial}{\partial r_{1z}}P(\vec{r}_1,\vec{r}_2)\frac{\partial}{\partial r_{2z}}P(\vec{r}_2,\vec{r}) = \sum_{m,m'} \frac{M_{mm'}M_{m'm}}{\tilde{\lambda}_{m'}\tilde{\lambda}_{m^2}} , \tag{A21}$$

where

$$M_{mm'} = \int d\vec{r}_1\, Q_m(\vec{r}_1)\frac{\partial}{\partial r_{1z}}Q^*_{m'}(\vec{r}_1) . \tag{A22}$$

In deriving Eq. (A21) we have used Eq. (A7) and performed the r integration using orthogonality. However, the presence of the derivative $\partial/\partial r_z$ leads us to the matrix elements $M_{mm'}$ which are not diagonal in m,m'. With use of Eq. (A9) it can be evaluated in a straightforward way, yielding

$$M_{m,m'} = \begin{cases} \dfrac{4m_z m_{z'}}{L_z[m_z^2-(m_z')^2]}\delta_{m_x,m_x'}\delta_{m_y,m_y'} & \text{if } m_z - m_z' \text{ odd} \\ 0 \text{ if } m_z - m_z' \text{ even} . \end{cases} \tag{A23}$$

Combining Eqs. (A19), (A20), and (A21), we finally obtain

$$F^{(\mathrm{ph})}_{5(\mathrm{b})} = -8\left[\frac{4}{\pi^2}\right]^2 \mathrm{Re}\left[\sum_{m_x,m_y=0}^{\infty}{\sum_{m_z=1}}'{\sum_{n_z=2}}'\frac{f_{mn}^2}{\tilde{\lambda}_m\tilde{\lambda}_n}\left[\frac{1}{\tilde{\lambda}_m}+\frac{1}{\tilde{\lambda}_n}\right]\right] , \tag{A24}$$

where $f_{mn} = 4m_z n_z/\pi(m_z^2-n_z^2)$, and the primes denote sums over even or odd integers only.

The evaluation of the four-diffusion diagram [Fig. 5(c)] proceeds in the same way. Now only the matrix element j_1 appears and we obtain

$$F^{(\mathrm{ph})}_{5(\mathrm{c})} = 24\left[\frac{4}{\pi^2}\right]^2 \mathrm{Re}\left[\sum_{m_x,m_y=0}^{\infty}{\sum_{m_z,p_z=1}}'{\sum_{n_z,q_z=2}}'\frac{f_{mn}f_{np}f_{pq}f_{qm}}{\tilde{\lambda}_m\tilde{\lambda}_n\tilde{\lambda}_p\tilde{\lambda}_q}\right] . \tag{A25}$$

Finally we consider Figs. 5(d) and 5(e). The integration associated with the current vertices is isolated and shown in Figs. 14(c) and 14(d). These are vertices of the type considered by Hikami[80] who showed that Figs. 14(c) and 14(d) cancel each other in the limit of zero external momentum. Thus Figs. 5(d) and 5(e) are not as divergent as Figs. 5(a)–5(c) and will be ignored.

Thus we obtain the total particle-hole contribution to the conductance fluctuation as follows:

$$F^{(\mathrm{ph})}(\Delta E, \Delta B = 0) = F^{(\mathrm{ph})}_{5(\mathrm{a})} + F^{(\mathrm{ph})}_{5(\mathrm{b})} + F^{(\mathrm{ph})}_{5(\mathrm{c})} . \tag{A26}$$

So far we have restricted our consideration to the particle-hole diffusion channel. In the absence of a magnetic field or spin-orbit scattering, we can reverse the arrow in one of the loops in Figs. 5(a), 5(b), and 5(c) and obtain an equal contribution from the particle-hole channel, so that

$$F = 2F^{(\mathrm{ph})} . \tag{A27}$$

However, we expect the particle-particle contribution to be suppressed by a magnetic field. It turns out that both the particle-hole and particle-particle contributions are affected by spin-orbit and spin-flip scattering; detailed results are given in Appendix C. Equations (A26) and (A27) are equivalent to the basic results (2.8) and (2.9) given in the text.

Figures 5(a)–5(e) represent the most singular diagrams to lowest order in $(\varepsilon_F\tau)^{-1}$. They are the most singular (divergent for $d \leq 4$) because they maximize the number of diffusions carrying the same momentum. If we go beyond the lowest order in $(\varepsilon_F\tau)^{-1}$, diagrams such as Fig. 15 can be considered as a renormalization of the diffusion propagator by weak localization effects, and will lead to the replacement of the diffusion constant D by $D(1+(\varepsilon_F\tau)^{-1}L^{d-2})$. Such terms may lead to corrections to F only of the form $(\varepsilon_F\tau)^{-1}L^{d-2}$. However, the important point is that corrections of the form $(\varepsilon_F\tau)^{-1}L^{d-4}$ do not exist, because corrections of this type could be exponentiated near $d=4$ to give a different L dependence than the leading term. Thus we believe that the conclusion that conductance fluctuation is independent of sample size is correct as long as the sample size greatly exceeds the mean free path and is much less than the localization length.

APPENDIX B: FORMULATION AT FINITE TEMPERATURES

In this appendix Eq. (3.3) at $T \neq 0$ is derived by use of the conventional thermal Green-function technique. For

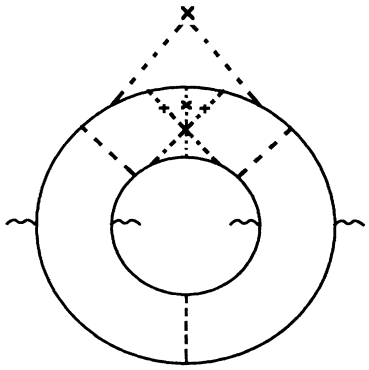

FIG. 15. An example of weak localization (maximally crossed diagram) correction to the conductance fluctuation diagram.

simplicity we assume here d-dimensional macroscopic systems so that we can work in the momentum representation. The effects of finite geometry, however, will easily be incorporated in the final results.

In order to calculate the correlation function of two static conductances, we first assign two different thermal frequencies, $\omega_\lambda(>0)$ and $\omega'_\lambda(>0)$, for external electric fields and extract the contributions in the order of $\omega_\lambda\omega'_\lambda$. it is to be noted that both types of processes shown in Figs. 16(a) and 16(b) as an example should be taken into account, where wiggly lines and dashed lines are current vertices and diffusion propagators. The contributions from Fig. 16(a) are given by

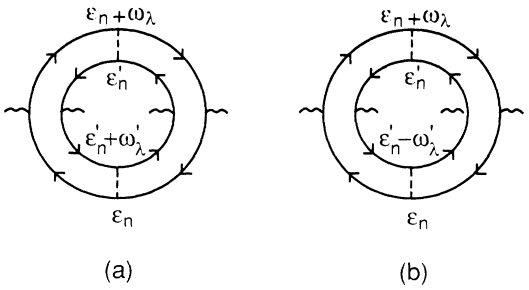

FIG. 16. Finite temperature version of Fig. 5(a).

$$A\sum_q T\sum_{\varepsilon_n>0} T\sum_{\varepsilon'_n>0}\left[\frac{2}{(Dq^2+\varepsilon_n+\varepsilon'_n)^4}+\frac{1}{Dq^2(Dq^2+\varepsilon_n+\varepsilon'_n)^3}\right], \tag{B1}$$

where A is defined as follows including the factor 4 coming from the summation over the spin indices of electrons:

$$A=16\tau^2\left[\frac{e}{m}\right]^4\left[\frac{k_F^2}{dL_z^2}\right]^2. \tag{B2}$$

The first term in expression (B1) results from the frequency regions satisfying $\varepsilon_n+\omega_\lambda>0$, $\varepsilon_n>0$, $\varepsilon'_n<0$, $\varepsilon'_n+\omega'_\lambda<0$ and $\varepsilon_n+\omega_\lambda<0$, $\varepsilon_n<0$, $\varepsilon'_n>0$, $\varepsilon'_n+\omega'_\lambda>0$, whereas the second term is due to the region of $\varepsilon_n+\omega_\lambda>0$, $\varepsilon_n<0$, $\varepsilon'_n<0$, $\varepsilon'_n+\omega'_\lambda>0$. For example, the derivation of the second term is as follows. Except for numerical factors it has the form

$$\begin{aligned} I&\equiv T\sum_{\varepsilon_n}{}' T\sum_{\varepsilon'_n}{}' \frac{1}{Dq^2+\varepsilon_n+\omega_\lambda-\varepsilon'_n}\frac{1}{Dq^2+\varepsilon'_n+\omega'_\lambda-\varepsilon_n} \\ &\equiv\frac{1}{2Dq^2+\omega_\lambda+\omega'_\lambda}T\sum_{\varepsilon_n}{}' T\sum_{\varepsilon'_n}\left[\frac{1}{Dq^2+\varepsilon_n+\omega_\lambda-\varepsilon'_n}+\frac{1}{Dq^2+\varepsilon'_n+\omega'_\lambda-\varepsilon_n}\right], \end{aligned} \tag{B3}$$

where the summations over ε_n and ε'_n are restricted in the regions $0>\varepsilon_n>-\omega_\lambda$, $0>\varepsilon'_n>-\omega'_\lambda$. Changing the signs of ε'_n and ε_n in the first and second terms in Eq. (B3), we obtain

$$I=\frac{2}{2Dq^2+\omega_\lambda+\omega'_\lambda}T\sum_{\omega_\lambda>\varepsilon_n>0} T\sum_{\omega'_\lambda>\varepsilon'_n>0}\frac{1}{Dq^2+\varepsilon_n+\varepsilon'_n}. \tag{B4}$$

By noting

$$T\sum_{\omega_\lambda>\varepsilon_n>0}\frac{1}{Dq^2+\varepsilon_n+\varepsilon'_n}=T\sum_{\varepsilon_n>0}\left[\frac{1}{Dq^2+\varepsilon_n+\varepsilon'_n}-\frac{1}{Dq^2+\varepsilon_n+\omega_\lambda+\varepsilon'_n}\right] \tag{B5}$$

and the similar relationship for the summation over ε'_n, we finally see that to the order of $\omega_\lambda\omega'_\lambda$

$$\begin{aligned} I&=\frac{4\omega_\lambda\omega'_\lambda}{2Dq^2+\omega_\lambda+\omega'_\lambda}T\sum_{\varepsilon_n>0} T\sum_{\varepsilon'_n>0}\frac{1}{(Dq^2+\varepsilon_n+\varepsilon'_n)^3} \\ &\cong\frac{2\omega_\lambda\omega'_\lambda}{Dq^2}T\sum_{\varepsilon_n>0} T\sum_{\varepsilon'_n>0}\frac{1}{(Dq^2+\varepsilon_n+\varepsilon'_n)^3}. \end{aligned} \tag{B6}$$

On the other hand, the contributions from Fig. 16(b) are given by

$$A\sum_q T\sum_{\varepsilon_n>0} T\sum_{\varepsilon'_n>0}\frac{1}{(Dq^2+\varepsilon_n+\varepsilon'_n)^4}. \tag{B7}$$

The sum of expressions (B1) and (B7) is rewritten as follows by analytic continuations of the thermal frequencies:

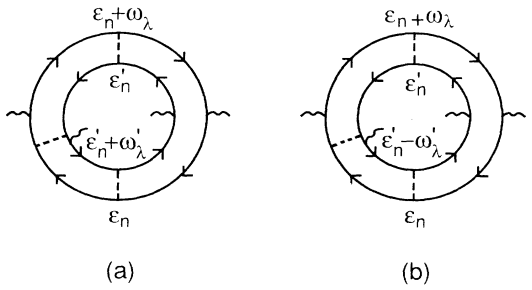

FIG. 17. Some of the finite-temperature version of the three diffusion diagrams [Fig. 5(b)].

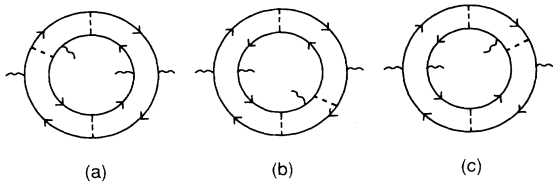

FIG. 18. More of the finite-temperature three-diffusion diagrams.

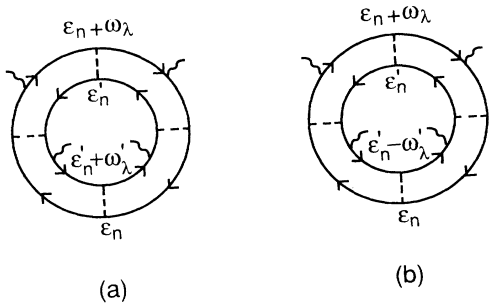

FIG. 19. Some of the finite-temperature versions of the form diffusion diagrams [Fig. 5(c)].

$$
\begin{aligned}
(\mathrm{B1})+(\mathrm{B7}) &= -\frac{A}{(2\pi)^2}\sum_q \int_{-\infty}^{\infty} dx \int_{-\infty}^{\infty} dx' f(x)f(x')\left[\frac{3}{[Dq^2-i(x+x')]^4}+\frac{1}{Dq^2[Dq^2-i(x+x')]^3}\right] \\
&= \frac{A}{2(2\pi)^2}\sum_q \int_{-\infty}^{\infty} dx \int_{-\infty}^{\infty} dx' f'(x)f'(x')\left[\frac{1}{[Dq^2-i(x+x')]^2}+\frac{1}{Dq^2}\frac{1}{[Dq^2-i(x+x')]}\right] \\
&= \frac{A}{4(2\pi)^2}\sum_q \int_{-\infty}^{\infty} d\omega\,\varphi(\omega)\left[\frac{1}{(Dq^2-i\omega)^2}+\frac{1}{(Dq^2+i\omega)^2}+\frac{2}{(Dq^2-i\omega)(Dq^2+i\omega)}\right] \\
&= \frac{A}{4(2\pi)^2}\sum_q \int_{-\infty}^{\infty} d\omega\,\varphi(\omega)\left[\frac{1}{Dq^2-i\omega}+\frac{1}{Dq^2+i\omega}\right]^2 ,
\end{aligned}
\tag{B8}
$$

where $f(x)=\{e^{\beta x}+1\}^{-1}$, β being $\beta=(kT)^{-1}$, $f'(x)=df(x)/dx$, and $\varphi(\omega)$ is defined by

$$
\varphi(\omega)=\int_{-\infty}^{\infty} dx\, f'(x)f'(\omega-x)\ . \tag{B9}
$$

The processes with three diffusions are treated similarly. Those shown in Figs. 17(a) and 17(b) result in

$$
\text{process [Fig. 17(a)]}+\text{process [Fig. 17(b)]} = -A\sum_q Dq^2 T\sum_{\varepsilon_n>0} T\sum_{\varepsilon'_n>0}(3+3+1+5)\frac{1}{(Dq^2+\varepsilon_n+\varepsilon'_n)^5}\ , \tag{B10}
$$

where numerical factors correspond to the contributions from the regions of $\varepsilon_n+\omega_\lambda>0$, $\varepsilon_n>0$, $\varepsilon'_n+\omega'_\lambda<0$, $\varepsilon'_n<0$ in Fig. 17(a); $\varepsilon_n+\omega_\lambda<0$, $\varepsilon_n<0$, $\varepsilon'_n+\omega'_\lambda>0$, $\varepsilon'_n>0$ in Fig. 17(a); $\varepsilon_n+\omega_\lambda>0$, $\varepsilon_n>0$, $\varepsilon'_n<0$, $\varepsilon'_n-\omega'_\lambda<0$ in Fig. 17(b); and $\varepsilon_n+\omega_\lambda<0$, $\varepsilon_n<0$, $\varepsilon'_n>0$, $\varepsilon'_n-\omega'_\lambda>0$ in Fig. 17(b), respectively. Each of the processes in Fig. 18 has the same contribution as Eq. (B10). Hence the three-diffusion processes result in

$$
-48A\sum_q T\sum_{\varepsilon_n>0} T\sum_{\varepsilon'_n>0}\frac{Dq^2}{(Dq^2+\varepsilon_n+\varepsilon'_n)^5} = -\frac{4A}{(2\pi)^2}\sum_q \int_{-\infty}^{\infty} d\omega\,\varphi(\omega)\,\mathrm{Re}\left[\frac{Dq^2}{(Dq^2-i\omega)^3}\right] . \tag{B11}
$$

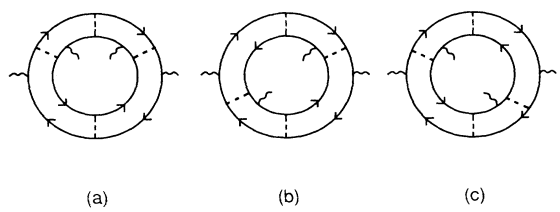

FIG. 20. More of the finite-temperature-form diffusion diagrams.

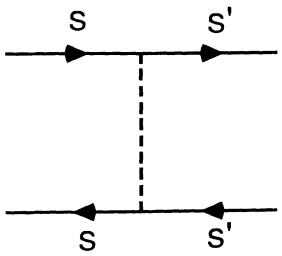

FIG. 21. The particle-hole diffusion channel which remains singular in the presence of spin-orbit scattering. The spin index is labeled by s and s'.

It is to be noted that there exist cancellations among processes with three diffusions, e.g., those shown in Fig. 19 where + (−) stands for positive (negative) thermal frequencies.

The processes with four diffusions are as follows. For example, the processes shown in Figs. 20(a) and 20(b) result in

$$2A\sum_q (Dq^2)^2 T\sum_{\varepsilon_n>0} T\sum_{\varepsilon_n'>0} (4+4+1+11) \times \frac{1}{(Dq^2+\varepsilon_n+\varepsilon_n')^6}, \tag{B12}$$

where numerical factors correspond to the contributions from the region of $\varepsilon_n+\omega_\lambda>0$, $\varepsilon_n>0$, $\varepsilon_n'+\omega_\lambda'<0$, $\varepsilon_n'<0$ in Fig. 20(a); $\varepsilon_n+\omega_\lambda<0$, $\varepsilon_n<0$, $\varepsilon_n'+\omega_\lambda'>0$, $\varepsilon_n'>0$ in Fig. 20(a); $\varepsilon_n+\omega_\lambda>0$, $\varepsilon_n>0$, $\varepsilon_n'+\omega_\lambda'<0$, $\varepsilon_n'<0$ in Fig. 20(b); and $\varepsilon_n+\omega_\lambda<0$, $\varepsilon_n<0$, $\varepsilon_n'+\omega_\lambda'>0$, $\varepsilon_n'>0$ in Fig. 20(b), respectively. The corresponding numerical factors coming from the processes shown in Figs. 21(a) and 21(b) are $(4+4+1+11)$ and $(5+5+5+5)$, respectively, and the total contribution from the four-diffusion processes are

$$120A\sum_q (Dq^2)^2 T\sum_{\varepsilon_n>0} T\sum_{\varepsilon_n'>0} \frac{1}{(Dq^2+\varepsilon_n+\varepsilon_n')^6} = \frac{6A}{(2\pi)^2}\sum_q \int_{-\infty}^{\infty} d\omega\,\varphi(\omega)\,\mathrm{Re}\left[\frac{(Dq^2)^2}{(Dq^2-i\omega)^4}\right]. \tag{B13}$$

It is to be noted that either Fig. 21(b) or Fig. 21(c) should be taken into account since they are identical.

Equations (B8), (B11), and (B13) lead to the convolution formula in Eq. (3.3).

APPENDIX C: EFFECTS OF SPIN-ORBIT SCATTERING AND PARAMAGNETIC IMPURITIES

In the weakly localized regime spin-orbit scattering, scattering by paramagnetic impurities, and mutual interactions are known to affect the quantum corrections to various physical quantities. These are examined for the correlation function of conductivities.

In the presence of strong spin-orbit scattering, i.e., $\tau_{SO}^{-1}\gg T$, τ_{SO} being the lifetime due to such scattering, only particular channels of diffusions shown in Fig. 21, where S and S' are independent, are singular,[81] and the prefactors of these diffusions are reduced by half compared to those in Appendix B. Hence compared to $\sum 1=4$ in normal impurity scattering we have $\sum_{s,s'}(\frac{1}{2})^2=1$, $\sum_{s,s',s''}(\frac{1}{2})^3=1$, $\sum_{s,s',s'',s'''}(\frac{1}{2})^4=1$ for two, three, and four diffusion processes, respectively; i.e., total contribution in this case is just a quarter of that found in Appendix B.

The scattering by paramagnetic impurities needs special care, since spin flipping processes entangling two electron loops are forbidden. This is because these two loops correspond to two different observations, between which there will be no memory of directions of paramagnetic impurities, and then only average magnetization can affect the correlation of conductivities. This implies that even in the absence of a magnetic field, all singular contributions (not just the particle-particle channel) are suppressed once $\tau_s^{-1}>T$, τ_s being the lifetime due to scattering by paramagnetic impurities. On the other hand, once the field gets strong enough that $g_s\mu_B H>T$, g_s being the g factors of paramagnetic impurities, half of the singular contributions in the absence of paramagnetic scattering will be recovered. Since the aperiodic magnetoconductance fluctuations persist to very high fields, and at typical experimental temperatures the spin-flip processes will be frozen out at fields below 1 T, magnetic impurities will usually not prevent the observation of the universal conductance fluctuations. This is very different from the weak localization effects, which are usually very difficult to detect in systems with magnetic impurities.

*Present address: Applied Physics Section, Yale University, P.O. Box 2157, New Haven, CT 06520-2159.

[1]R. A. Webb, S. Washburn, C. P. Umbach, and R. B. Laibowitz, in *Localization, Interaction and Transport Phenomena in Impure Metals*, edited by G. Bergmann, Y. Bruynseraede, and B. Kramer (Springer, Berlin, 1985); C. P. Umbach, S. Washburn, R. B. Laibowitz, and R. A. Webb, Phys. Rev. B **30**, 4048 (1984).

[2]G. Blonder, Bull. Am. Phys. Soc. **29**, 535 (1984).

[3]R. A. Webb, S. Washburn, C. P. Umbach, and R. B. Laibowitz, Phys. Rev. Lett. **54**, 2696 (1985).

[4]S. Washburn, C. P. Umbach, R. B. Laibowitz, and R. A. Webb, Phys. Rev. B **32**, 4789 (1985).

[5]V. Chandrasekhar, M. J. Rooks, S. Wind, and D. E. Prober, Phys. Rev. Lett. **55**, 1610 (1985).

[6]C. P. Umbach, C. Van Haesendonck, R. B. Laibowitz, S. Washburn, and R. A. Webb, Phys. Rev. Lett. **56**, 386 (1986).

[7]J. C. Licini, D. J. Bishop, M. A. Kastner, and J. Melngailis, Phys. Rev. Lett. **55**, 2987 (1985).

[8]R. G. Wheeler, K. K. Choi, A. Goel, R. Wisnieff, and D. E. Prober, Phys. Rev. Lett. **49**, 1674 (1982).

[9]W. J. Skocpol, L. D. Jackel, R. E. Howard, P. M. Mankiewich, and D. M. Tennant, Surf. Sci. (to be published); R. E. Howard, L. D. Jackel, P. M. Mankiewich, and W. J. Skocpol, Science **231**, 346 (1986); W. J. Skocpol, P. M. Mankiewich, R. E. Howard, L. D. Jackel, D. M. Tennant, and A. D. Stone, Phys. Rev. Lett. (to be published).

[10]S. B. Kaplan and A. Hartstein, Phys. Rev. Lett. **56**, 2403 (1986); R. A. Webb, A. B. Fowler, and A. Hartstein (unpublished).

[11]A. D. Stone, Phys. Rev. Lett. **54**, 2692 (1985).
[12]B. L. Al'tshuler, Pis'ma Zh. Eksp. Teor. Fiz. **51**, 530 (1985) [JETP Lett. **41**, 648 (1985)].
[13]P. A. Lee and A. D. Stone, Phys. Rev. Lett. **55**, 1622 (1985).
[14]B. L. Al'tshuler and D. E. Khmel'nitskii, Pis'ma Zh. Eksp. Teor. Fiz. **42**, 291 (1985) [JETP Lett. **42**, 359 (1986)].
[15]R. Landauer, IBM J. Res. Dev. **1**, 223 (1957); Philos. Mag. **21**, 863 (1970).
[16]P. W. Anderson, D. J. Thouless, E. Abrahams, and D. S. Fisher, Phys. Rev. B **22**, 3519 (1980).
[17]E. Abrahams and M. Stephen, J. Phys. C **13**, L377 (1980).
[18]B. Andereck and E. Abrahams, J. Phys. C **13**, 1383 (1980).
[19]A. D. Stone, J. D. Joannopoulos, and D. J. Chadi, Phys. Rev. B **24**, 5583 (1981).
[20]A. D. Stone and J. D. Joannopoulos, Phys. Rev. B **25**, 1431 (1982).
[21]I. M. Lifshitz and V. Ya. Kirpichenkov, Zh. Eksp. Teor. Fiz. **77**, 989 (1979) [Sov. Phys.—JETP **50**, 499 (1979)].
[22]M. Ya. Azbel, Solid State Commun. **45**, 527 (1983).
[23]M. Ya. Azbel, A. Hartstein, and D. P. DiVincenzo, Phys. Rev. Lett. **52**, 1641 (1984), and references therein.
[24]The arguments which predict large statistical fluctuations in g for a fixed energy, E, are typically derived by excluding configurations for which E is an eigenvalue. Thus the large fluctuations in g arise from small fluctuations in $\ln g$ (or equivalently, the inverse localization length) from configuration to configuration; the fluctuations in g versus E in a given sample seem to be primarily due to resonances and not due to fluctuations in the inverse localization length as a function of energy away from a resonance. Therefore it is not at all clear that $g(E)$ in the strongly-localized regime will have identical fluctuations as those from sample to sample, although both are certainly expected to have large fluctuations. As noted later, the physical basis for our ergodic hypothesis relating magnetic field fluctuations to statistical fluctuations may also break down in the strongly-localized regime, so the apparent validity of our ergodic hypothesis in the metallic regime is not trivial.
[25]A. B. Fowler, A. Hartstein, and R. A. Webb, Phys. Rev. Lett. **48**, 196 (1982).
[26]R. A. Webb, A. Hartstein, J. J. Wainer, and A. B. Fowler, Phys. Rev. Lett. **54**, 1577 (1985).
[27]P. A. Lee, Phys. Rev. Lett. **52**, 1641 (1984); A. D. Stone and P. A. Lee, *ibid.* **54**, 1196 (1985).
[28]D. J. Thouless, Phys. Rev. Lett. **39**, 1167 (1977).
[29]E. Abrahams, P. W. Anderson, D. C. Licciardello, and T. V. Ramakrishnan, Phys. Rev. Lett. **42**, 673 (1979).
[30]D. J. Thouless, J. Phys. C **6**, L49 (1973).
[31]D. S. Fisher and P. A. Lee, Phys. Rev. B **23**, 6851 (1981).
[32]D. C. Langreth and E. Abrahams, Phys. Rev. B **31**, 2978 (1981).
[33]M. Ya. Azbel, J. Phys. C **14**, L225 (1981).
[34]M. Büttiker, Y. Imry, R. Landauer, and S. Pinhas, Phys. Rev. B **31**, 6207 (1985).
[35]R. Landauer, in *Localization, Interaction and Transport Phenomena in Impure Metals,* edited by G. Bergmann, Y. Bruynseraede, and B. Kramer (Springer, Berlin, 1985).
[36]N. Bohr, Nature **137**, 344 (1936).
[37]E. P. Wigner, Ann. Math. **53**, 36 (1953); **62**, 548 (1955); **65**, 203 (1957); **67**, 325 (1958).
[38]F. J. Dyson, J. Math. Phys. **3**, 140 (1962); **3**, 157 (1962); **3**, 166 (1962); F. J. Dyson and M. L. Mehta, J. Math. Phys. **4**, 701 (1963).
[39]For a good review of applications of random matrix theory to nuclear spectra see T. A. Brody, J. Flores, J. B. French, P. A. Mello, A. Pandey, and S. S. M. Wong, Rev. Mod. Phys. **53**, 385 (1981).
[40]T. Ericson and T. Mayer-Kuckuk, Ann. Rev. Nucl. Sci. **16**, 183 (1966).
[41]Y. Imry, Europhysics Lett. **1**, 249 (1986).
[42]B. L. Al'tshuler and B. I. Shklovskii (unpublished).
[43]The energy interval over which the spectrum exhibits spectral rigidity is just $E_c = hD/L^2$, the energy correlation range derived in Refs. 13, 47, and 59, as discussed in the text.
[44]S. Feng, P. A. Lee, and A. D. Stone, Phys. Rev. Lett. **56**, 1960 (9186); **56**, 2772(E) (1986).
[45]Y. Gefen, Y. Imry, and M. Ya. Azbel, Phys. Rev. Lett. **52**, 129 (1984).
[46]A. D. Stone, P. A. Lee, and D. DiVincenzo (unpublished).
[47]A. D. Stone and Y. Imry, Phys. Rev. Lett. **56**, 189 (1986).
[48]E. Abrahams, P. W. Anderson, P. A. Lee, and T. V. Ramakrishnan, Phys. Rev. B **24**, 6783 (1981).
[49]See, for example, L. S. Schulman, *Techniques and Applications of Path Integration* (Wiley, New York, 1981), Chap. 18.
[50]D. E. Khmelnitskii and A. I. Larkin, Usp. Fiz. Nauk. **136**, 533 (1982) [Sov. Phys.—Usp. **25**, 185 (1982)].
[51]S. Chakravarty and A. Schmid, Phys. Rep. (to be published).
[52]G. Bergmann, Phys. Rep. **107**, 11 (1984).
[53]B. L. Al'tshuler, A. G. Aronov, and B. Z. Spivak, Pis'ma Zh. Eksp. Teor. Fiz. **33**, 101 (1981) [JETP Lett. **33**, 94 (1981)].
[54]D. Yu. Sharvin and Yu. V. Sharvin, Pis'ma Zh. Eksp. Teor. Fiz. **34**, 285 (1981) [JETP Lett. **34**, 272 (1981)].
[55]M. Murat, Y. Gefen, and Y. Imry, Phys. Rev. B **34**, 659 (1986).
[56]Although there is a systematic perturbation expansion for g in the small parameter $(k_F l)^{-1}$, the coefficients in that expansion are divergent for $d \leq 2$. This observation was an important justification of the result implied by the scaling theory of localization that all states are localized for any degree of disorder in these dimensions (see Ref. 29).
[57]P. A. Lee and D. S. Fisher, Phys. Rev. Lett. **47**, 882 (1981).
[58]See, for example, A. A. Abrikosov, L. P. Gorkov, and I. E. Dzyaloshinski, *Methods of Quantum Field Theory in Statistical Physics* (Prentice-Hall, Englewood Cliffs, 1963), Chap. 7, Sec. 39.2.
[59]P. F. Maldague, Phys. Rev. B **23**, 1719 (1981).
[60]B. L. Al'tshuler, D. E. Khmelnitzskii, A. I. Larkin, and P. A. Lee, Phys. Rev. B **22**, 5142 (1980).
[61]M. Büttiker and Y. Imry, J. Phys. C **18**, L467 (1985).
[62]B. L. Al'tshuler and B. Z. Spivak, Pis'ma Zh. Eksp. Teor. Fiz. **42**, 363 (1985) [JETP Lett. **42**, 447 (1986)].
[63]M. Ma and P. A. Lee (unpublished).
[64]M. Büttiker (unpublished).
[65]A. D. Benoit, S. Washburn, C. P. Umbach, R. B. Laibowitz, and R. A. Webb (unpublished).
[66]See P. A. Lee and T. V. Ramakrishnan, Rev. Mod. Phys. **57**, 287 (1985) for a review.
[67]H. Fukuyama and E. Abrahams, Phys. Rev. B **27**, 5976 (1983); H. Fukuyama, in *Localization, Interaction and Transport Phenomena in Impure Metals,* edited by G. Bergmann, Y. Bruynseraede, and B. Kramer (Springer, Berlin, 1985).
[68]C. Castellani, C. DiCastro, G. Kotliar, and P. A. Lee, Phys. Rev. Lett. **56**, 1179 (1986).
[69]A. Schmid, Z. Phys. **259**, 421 (1973).
[70]B. L. Al'tshuler, A. G. Aronov, and D. E. Khmelnitzskii, J. Phys. C **15**, 7367 (1982).
[71]D. J. Thouless, J. Non-Cryst. Solids **35/36**, 3 (1980).
[72]In fact, early numerical studies of the scaling of the average

conductance with size near the metal-insulator transition gave size-independent error bars from which the magnitude of the universal conductance fluctuations can be obtained (see Ref. 56).

[73]J. W. Goodman, J. Opt. Soc. Am. **66**, 1145 (1976).

[74]S. Feng, P. A. Lee, and A. D. Stone (unpublished).

[75]M. Stephen, Phys. Rev. Lett. **56**, 1809 (1986), and references therein.

[76]M. P. Van Albada and A. Lagendijk, Phys. Rev. Lett. **55**, 2692 (1985).

[77]P. E. Wolf and G. Maret, Phys. Rev. Lett. **55**, 2696 (1985).

[78]In Ref. 44 it was incorrectly stated that the rms change induced by moving a single strong scatterer in two dimensions would be of order e^2/h for any metal, independent of disorder. The effect is indeed size independent in two dimensions, but decreases with decreasing disorder in the manner stated in the text. The numerical calculations done to confirm the analytic results in Ref. 44 were done for $k_F l \sim 1$ and hence, while correct, did not reveal the error. More detailed corrections are given in an erratum, Phys. Rev. Lett. **56**, 2772(E) (1986).

[79]H. E. Engquist and P. W. Anderson, Phys. Rev. B **24**, 1151 (1981).

[80]S. Hikami, Phys. Rev. B **24**, 2671 (1981).

[81]H. Fukuyama, J. Phys. Soc. Jpn. **51**, 1105 (1982).